A comprehensive global three-dimensional model of delta O-18 in atmospheric CO2: 1. Validation of surface processes

Matthias Cuntz, Philippe Ciais, Gilles Hoffmann, W. Knorr

A comprehensive global three-dimensional model of $\delta^{18}O$ in atmospheric CO_2:
1. Validation of surface processes

Matthias Cuntz

Laboratoire des Sciences du Climat et de l'Environnement, Unité Mixte de CNRS/CEA, Gif-sur-Yvette, France
Institut für Umweltphysik, Universität Heidelberg, Heidelberg, Germany

Philippe Ciais and Georg Hoffmann

Laboratoire des Sciences du Climat et de l'Environnement, Unité Mixte de CNRS/CEA, Gif-sur-Yvette, France

Wolfgang Knorr

Max-Planck-Institut für Biogeochemie, Jena, Germany

[1]   We have built the first comprehensive global three-dimensional model of $\delta^{18}O$ in atmospheric CO_2. The constructed model goes beyond all other approaches made until now, by simulating the diurnal variations and transport of CO_2, $\delta^{18}O$ of water, and $\delta^{18}O$ of CO_2. The $CO^{18}O$ fluxes are thereby dependent on the atmospheric $CO^{18}O$ composition. We have validated the model surface processes, showing that it compares well to other estimates and measurements of NPP, NEE, and stomata-internal CO_2 mixing ratio (c_i), except for high northern latitudes. Here, the model is considerably lower in NPP and higher in c_i than other model estimates. However, estimates derived indirectly from observations tend to support our model findings. The water isotopes of rain are reproduced very well at all latitudes. The soil bucket model used in the model integrates incoming rain in one single value. The bucket approach overattenuates the isotopic variations of rain, and hence our isotopic source signature of respiration shows almost no seasonal cycle and is thus isotopically too depleted during summer.   *INDEX TERMS:* 0315 Atmospheric Composition and Structure: Biosphere/atmosphere interactions; 0322 Atmospheric Composition and Structure: Constituent sources and sinks; 1610 Global Change: Atmosphere (0315, 0325); 1615 Global Change: Biogeochemical processes (4805); 3210 Mathematical Geophysics: Modeling; *KEYWORDS:* isotope model, ^{18}O in CO_2, ^{18}O in H_2O, ecosystem model, biosphere-atmosphere exchange, isotope discrimination

Citation: Cuntz, M., P. Ciais, G. Hoffmann, and W. Knorr, A comprehensive global three-dimensional model of $\delta^{18}O$ in atmospheric CO_2: 1. Validation of surface processes, *J. Geophys. Res.*, *108*(D17), 4527, doi:10.1029/2002JD003153, 2003.

1.   Introduction

[2]   The atmospheric signal of CO_2 is an integrated measure of all processes adding CO_2 to and removing CO_2 from the atmosphere. Consequently, one can deduce only the net CO_2 flux from atmospheric measurements. Inversion studies of atmospheric CO_2 measurements make therefore only predictions of net CO_2 fluxes over different regions [e.g., *Gurney et al.*, 2002]. To separate the different components of the net flux, several tracers are used, depending on the component. For example, ^{13}C is used to differentiate between ocean and terrestrial biosphere fluxes, or ^{14}C is used to separate the fossil fuel combustion component. ^{18}O offers the possibility to separate the different terrestrial biospheric gross fluxes, namely assimilation and respiration. This is because CO_2 can exchange ^{18}O atoms with two isotopically distinct water pools, either with leaf

water or with soil water. Statistically, a CO_2 molecule going into plant leaves is fixed by photosynthesis with a probability of 1/3 whereas it diffuses back to the atmosphere with a probability of 2/3. Nevertheless, the isotopic exchange between CO_2 and water within leaves in the presence of the enzyme carbonic anhydrase is so fast that back-diffused CO_2 re-entering the atmosphere is isotopically "tagged" by evaporating leaf water. Leaf water at the evaporating site is generally significantly enriched with respect to soil moisture and so is leaf CO_2 with respect to soil respired CO_2. However, unlike the case of ^{13}C, where the ocean, C_4 plants, and C_3 plants have distinct, narrowly defined signatures that are similar all over the globe, the ^{18}O isotopic labeling of CO_2 by photosynthesis and respiration varies in space and time, reflecting hydrological processes and climate-dependent fractionation factors. This means that in order to understand the integrated atmospheric signal of ^{18}O in CO_2, one must use a spatially explicit model of surface fluxes bound to a three-dimensional model of the atmospheric transport including water isotopic composition.

[3] Few studies have attempted so far to model the distribution of ^{18}O in atmospheric CO$_2$. The major conceptual difficulty lies in the requirement of a triad of models describing (1) the gross carbon fluxes, (2) the water isotope variability, and (3) the atmospheric transport. *Ciais et al.* [1997a, 1997b] have put together those three components using output from different published models that were sampled as monthly averages. This approach gave a reasonably good comparison with atmospheric observations and provided useful a priori estimates to inverse modeling of the gross fluxes [*Peylin*, 1999], but it remains unsatisfactory for three reasons: First, there were inconsistencies among the different models that were used to construct CO^{18}O fluxes inducing systematic errors that are impossible to estimate. Second, working with monthly mean fluxes does not permit proper up-scaling of biogeochemical processes from the ecosystem level up to the quasi global atmospheric signal. Third, working with monthly fluxes neglects the existence of a strong daily cycle in the fluxes of photosynthesis and respiration that unfortunately covary with atmospheric transport in the boundary layer to generate mean gradients in CO$_2$ and in δ^{18}O-CO$_2$.

[4] In this paper, we present a new, comprehensive model of ^{18}O in atmospheric CO$_2$ where leaf and soil processes that determine the isotopic fluxes are encapsulated into a land surface carbon flux model, interfaced to a global atmospheric circulation model. The CO$_2$ and CO^{18}O flux model is described in section 2, and its results are compared against ground based, pointwise CO$_2$ flux measurements and isotopic data in section 3. A companion paper is devoted to the comparison between background measurements of CO$_2$ and δ^{18}O-CO$_2$ in flask samples and the modeled δ^{18}O-CO$_2$ values obtained by atmospheric transport acting on surface sources [*Cuntz et al.*, 2003] (hereinafter referred to as part 2).

2. Model Description

[5] The model, named ECHAM/BETHY or BETHY online, includes four parts, which are shown in Figure 1. ECHAM is the Atmospheric General Circulation Model (AGCM) within which are embedded the calculations for the isotopic composition of different water reservoirs (WFRAC), as well as the atmospheric tracer transport. BETHY is a biosphere model which is driven with variables from ECHAM; it releases its calculated CO$_2$ surface fluxes into the ECHAM atmosphere. OFRAC is the CO^{18}O flux module which takes ECHAM and BETHY variables and the δ^{18}O value of CO$_2$ in the ECHAM atmosphere to calculate CO^{18}O fluxes which are emitted in the atmosphere of ECHAM. Later, we will describe the different parts of the model. We introduce ECHAM and WFRAC only briefly because they are described in detail elsewhere [*Modellbetreuungsgruppe*, 1994; *Hoffmann et al.*, 1998]. Extensive descriptions of BETHY are given by *Knorr* [1997, 2000] and *Knorr and Heimann* [2001a, 2001b] but we describe the main aspects that influence the calculations of CO^{18}O fluxes. OFRAC is based on the equations of *Ciais et al.* [1997a], which were adapted to calculate the CO^{18}O fluxes online in an AGCM. We explain them in detail to elaborate on the differences between ECHAM/ BETHY and earlier δ^{18}O-CO$_2$ models.
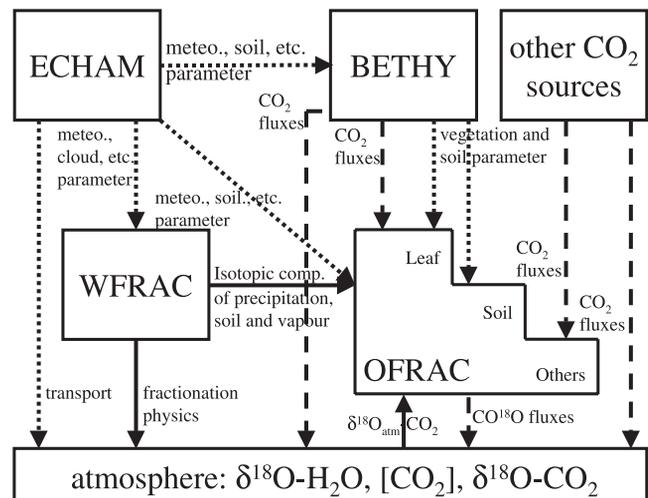
Figure 1. Interactions between the different parts of the model. ECHAM is the AGCM in which the water isotopes (WFRAC) and the tracer transport are included. BETHY is interfaced and the CO^{18}O isotope module (OFRAC) is 'coupled' to ECHAM. Solid lines stand for isotopic processes, dashed lines stand for CO$_2$ and CO^{18}O fluxes and dotted lines stand for physical and meteorological parameters, and for transport.

[6] ECHAM is a state-of-the-art AGCM that has been used in several studies [e.g., *Arpe et al.*, 1994; *Roeckner et al.*, 1992]. In this study, we used the T21 spectral truncation scheme, which corresponds to a physical grid of $5.6° \times 5.6°$ (time step of 40 minutes). The model has 19 vertical layers from surface pressure up to a pressure level of 30 hPa and includes a tracer transport scheme. WFRAC is implemented in ECHAM, and calculates for each phase of "normal" water, H$_2$O, two isotopic counterparts, H$_2^{18}$O and HDO. It has shown its excellent capability to simulate recent, paleo water and snow isotope distributions in a variety of studies [e.g., *Hoffmann et al.*, 1998, 2000; *Werner et al.*, 2001].

2.1. The CO$_2$ Flux Model BETHY

[7] We interfaced a process-based model of terrestrial vegetation activity, the Biosphere Energy—Transfer Hydrology scheme (BETHY) to the AGCM ECHAM. BETHY calculates CO$_2$ fluxes of the terrestrial biosphere, together with additional diagnostic variables for the biosphere, e.g., stomatal conductance and vegetation temperature. For BETHY offline model descriptions please refer to *Knorr* [1997, 2000] and *Knorr and Heimann* [2001a, 2001b]. We interfaced BETHY rather than coupling it to ECHAM; this will be done in a future step. That means that BETHY online does not interfere in the AGCM ECHAM. BETHY online is forced by meteorological variables of ECHAM but ECHAM is not influenced by BETHY. In addition, BETHY uses its own land-surface scheme. Therefore in order to obtain realistic evapotranspiration rates, vegetation temperatures and, hence, realistic stomatal conductances from the ECHAM energy and water budgets, we recompute the latent and sensible heat fluxes from the canopy of BETHY (even if they are already computed by ECHAM with its internal land surface scheme). Since plants lose water through their sto-

Table 1. List of Plant Functional Types Used in the BETHY Online Model With Assigned Parameters[a]

	Plant Functional Types[b]	V_m	J_m/k	h_V	C_4
1	Trop. BL E trees	60	118	30.0	
2	Trop. BL D trees	90	179	15.0	
3	Temp. BL E trees	41	82	15.0	
4	Temp. BL D trees	35	70	15.0	
5	E coniferous trees	29	52	15.0	
6	D coniferous trees	53	95	15.0	
7	E shrubs	52	102	1.0	
8	D shrubs	160	266	1.0	
9	C_3 short grass	42	80	0.3	
10	C_3 long grass	42	80	2.0	
11	C_4 short grass	8	140	0.3	x
12	C_4 long grass	8	140	2.0	x
13	Tundra vegetation	20	37	0.3	
14	Swamp vegetation	20	37	0.3	
15	Arable crops	117	220	0.6	
16	Irrigated crops	123	227	0.6	
17	Tropical tree crops	60	106	2.0	
18	Citrus crops	60	106	2.0	
19	Temp. D tree crops	123	227	2.0	
20	Sugar cane	39	700	2.0	x
21	Maize	39	700	2.0	x
22	Rice	98	190	0.3	
23	Cotton	123	227	1.0	

   [a]V_m, maximum carboxylation rate at 25°C in mol(CO₂) m⁻² s⁻¹; J_m, maximum electron transport rate at 25°C in mol(CO₂) m⁻² s⁻¹ (C₃), or k, PEPcase rate constant for CO₂ at 25°C (and standard pressure) in mol(CO₂) m⁻² s⁻¹ (C₄); h_V, height in m; C₄, using C₄ photosynthetic pathway instead of C₃.

   [b]Abbreviations: Trop., tropical; Temp., temperate; BL, broad-leaved; E, evergreen; D, deciduous.

matal pores while photosynthesizing, water availability is related closely to carbon uptake.

[8] The relationship between canopy net assimilation rate F_A (gross assimilation rate, "GPP", minus leaf respiration, F_{Rleaf}), canopy conductance g_c (integral over stomatal conductances g_s), and stomata-internal CO₂ mixing ratio c_i is:

$$F_A = g_c(c_a - c_i) \qquad (1)$$

where c_a is the mixing ratio of atmospheric CO₂ in ppm = mol(CO₂)/mol(air) and g_c is expressed in mol(CO₂) m² s⁻¹. The photosynthesis part of the model computes absorption of photosynthetically active radiation (PAR) through the canopy with a two-flux scheme [*Sellers*, 1985] for three vertical layers of equal LAI, gross carbon uptake, and leaf respiration. Carbon uptake and leaf respiration are described with the so-called Farquhar model for C₃ [*Farquhar et al.*, 1980] and a similar model for C₄ plants [*Collatz et al.*, 1992]. These are process-oriented models which require a rather large number of kinetic and structural parameters. Plant functional types used, together with the assigned parameters are shown in Table 1. To describe the stomatal response to environmental factors a semi-empirical approach is used, with only one free parameter. Observations suggest that in the absence of water limitation, canopy conductance is determined by photosynthetic demand for CO₂ [*Schulze et al.*, 1994]. So a non-water-stressed canopy conductance, g_{c0}, is first computed at a standard non-water-stressed stomata-internal CO₂ mixing ratio, c_{i0} [*Jones*, 1983; *Knorr*, 1997]:

$$g_{c0} = \frac{F_{A0}}{c_a - c_{i0}} \qquad (2)$$

where F_{A0} is the non-water-limited net leaf CO₂ uptake in mol(CO₂) m⁻² s⁻¹ and g_{c0} is given in mol(CO₂) m⁻² s⁻¹. If

photosynthesis is limited by availability of soil water, stomata are assured to close, in response to air vapor pressure deficit, Δe [*Schulze et al.*, 1987; *Schulze*, 1986; *Turner*, 1986; *Fischer and Turner*, 1978]. We use the empirical formula [*Lindroth and Halldin*, 1986]:

$$g_c = g_{c0} \frac{1}{1 + b_e \Delta e}. \qquad (3)$$

The factor b_e is assumed to change such that transpiration through the stomate does not exceed the root supply rate, S [*Federer*, 1982]:

$$S = c_w \frac{W_s}{W_{s,max}} \qquad (4)$$

where W_s is the soil water content adjusted to take soil freezing into account, $W_{s,max}$ the maximal root available soil water content and c_w an empirical parameter representing root density. We adopted a value of $c_w = 0.5$ mm/hour from a comparison with measured values of F_A and g_c for single days [*Knorr*, 1997] and a global sensitivity study on this parameter [*Knorr and Heimann*, 2001a].

[9] The computational and logical steps are as follows: the BETHY online model first calculates F_A as F_{A0} from the Farquhar model using c_{i0}. The non-water-stressed canopy conductance, g_{c0}, is then computed from equation (2) (at $c_i = c_{i0}$). After determining g_c from equation (3), the Farquhar model is resolved with unknown c_i but with the additional constraint that equation (1) must be satisfied.

[10] There are several descriptions of heterotrophic or soil respiration [*Raich and Potter*, 1995; *Lloyd and Taylor*, 1994; *Raich and Schlesinger*, 1992; *Meentemeyer*, 1978] that have in common that soil respiration approximately follows temperature, and that micro-organisms need water to produce CO₂. We use the formulation of *Raich and Potter* [1995] with $Q_{10} = 1.5$ and 2 m air temperature, T_a, because this smaller value is more consistent with the observed seasonal cycle of atmospheric CO₂ [*Knorr and Heimann*, 1995] compared to the more 'traditional' value of $Q_{10} = 2.0$ [*Raich and Schlesinger*, 1992]. Furthermore, we include a proportional dependence on actual over potential evapotranspiration, f_e [*Meentemeyer*, 1978]:

$$F_{Rhet} = c_1 f_e Q_{10}^{T_a/10} \qquad (5)$$

where

$$f_e = \frac{E_v}{E_{vmax}}. \qquad (6)$$

E_v is the actual and E_{vmax} the maximum possible transpiration rate from soil and vegetation. The rate c_1 is renormalized such that the mean of F_{Rhet} over 10 years equals the mean of NPP at every grid point; i.e., the terrestrial biosphere is supposed to be in equilibrium.

[11] The BETHY online version does not include a phenology scheme but rather it is taken as monthly input from the offline version of BETHY optimized with satellite-derived fraction of photosynthetically active radiation absorbed by vegetation (FPAR) [*Knorr and Heimann*, 2001b].

2.2. Nonbiospheric CO₂ Fluxes

[12] *Ciais et al.* [1997b] stated that one needs biomass burning and fossil fuel emissions to model a more realistic

north-south gradient of δ^{18}O-CO$_2$. Hence we introduce into the atmosphere nonbiospheric CO$_2$ fluxes from linear interpolation between monthly mean input fields. First, we take the formulation of *Wanninkhof* [1992] to compute the air-sea gas exchange coefficient and the instantaneous ECHAM wind fields to calculate CO$_2$ ocean fluxes from the ocean ΔpCO$_2$ compilation of *Takahashi et al.* [1999]. Second, we include fossil fuel CO$_2$ emissions via the annual compilation of *Andres et al.* [1996] which we distributed on a monthly basis with coefficients given by *Marland et al.* [1998]. Further, we introduce biomass burning emissions into the atmosphere. These include forest and savannah burning (seasonal) and agricultural wastes and fuel wood burning (annually constant) [*Hao and Liu*, 1994]. All fluxes are scaled to values representative of the year 1990. However, regrowth after burning is not included in the online version of BETHY, and we have no closed carbon cycle, though, respiration is supposed to be in equilibrium with assimilation. One can see below in equation (23) that the δ^{18}O-CO$_2$ cycle depends on gross biospheric fluxes which are at least one order of magnitude higher than the net biospheric fluxes and especially the missing fluxes required to close the carbon cycle in the model.

2.3. The CO^{18}O Flux Module OFRAC

[13] The δ^{18}O isotopic signature of CO$_2$ is determined mainly by the isotopic equilibrium reaction:

$$COO + H_2^{18}O \leftrightarrow CO\,^{18}O + H_2O. \qquad (7)$$
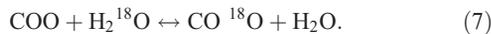
If this reaction occurs in nature, in most cases there are several orders of magnitude more water associated than CO$_2$. That means that the isotopic signature of CO$_2$ is fully determined by the isotopic signature of the equilibrating water which is barely changing itself. This equilibration process is temperature dependent, and the fractionation follows the relationship [*Brenninkmeijer et al.*, 1983]:

$$\epsilon_{eq}(T) = \left(\frac{17604}{T} - 17.93\right)/1000, \qquad (8)$$

where

$$\alpha_{eq}(T) = 1 + \epsilon_{eq}(T) \qquad (9)$$

is the fractionation factor. For example, the fractionation at 25°C is: ϵ_{eq} = +41.1‰ and dϵ_{eq}/dT = -0.2‰ °C^{-1}. This implies that higher temperatures lead to more depleted δ^{18}O-CO$_2$ values with constant δ^{18}O-H$_2$O. The isotope ratio of CO$_2$, R, equilibrated with water of composition R^W is hence: $R = \alpha_{eq}(T)\,R^W$. The rate of isotopic equilibration, $^{18}k_H$, is thereby one third as fast as the rate of hydration of CO$_2$ in water, k_H, because there are three oxygen atoms involved in reaction 7 and only one oxygen atom comes from H$_2$O. k_H is 0.0062 s^{-1} at 20°C [*Stern et al.*, 1999] and $^{18}k_H$ is therefore 0.0021 s^{-1}. This means that the e-folding time of hydration is lower than 3 min (with the Bunsen solubility close to 1, which is true for CO$_2$ and if the entry of CO$_2$ into water is not rate limiting) and the e-folding time of isotopic equilibration is about 8 min. CO$_2$ is thus equilibrated isotopically with ocean water, and with soil water in a certain depth (on the order of 10 cm). The

enzyme carbonic anhydrase present in leaf water speeds up the reaction rate by a factor of 10^7 [*Stryer*, 1981] so that CO$_2$ is also equilibrated isotopically with leaf water. However, the e-folding time is too long for CO$_2$ to hydrate in cloud droplets and more than ever too long to equilibrate isotopically with cloud water [*Francey and Tans*, 1987].

[14] A flux of CO$_2$ from one contributing process, F, is accompanied by a flux of CO^{18}O, ^{18}F. If there are exchanges of CO$_2$ between two compartments, pools or reservoirs, or if there is a phase transition, a fractionation occurs because of differing diffusivities (α can be higher, lower or equal to 1). For example, the complex phenomenon of diffusion out of the soil is accompanied by just one fractionation factor in our model. The CO^{18}O flux is calculated therefore as:

$$^{18}F = \alpha\,\alpha_{eq}(T)R^W F \qquad (10)$$

where α represents the fractionation occurring at the transition from one compartment or phase into another.

[15] Our CO$_2$ fluxes are supposed to be C^{16}O^{16}O fluxes alone and not the sum of C^{16}O^{16}O and C^{16}O^{18}O flux. This overestimates F by about 0.4% (the natural abundance of ^{18}O is approximately 0.2% [*Firestone et al.*, 1999]) which is negligible. Treating F as C^{16}O^{16}O and C^{16}O^{18}O flux would require to recompute α's and R's which are measured quantities and therefore the ratios of ^{18}O to ^{16}O concentrations (and not ^{18}O to ^{18}O plus ^{16}O). For example, this would change the soil fractionation ϵ_s (see below), which is taken here as -7.20‰, to -7.19‰. The recomputation would change our ^{18}F fluxes by approximately 0.2%, which leads to a change in δ of 0.02‰. Recomputation would not lead to perceptible changes in the results so that we discard recomputation for simplicity. We would also like to point out that all tracers are calculated as CO$_2$ and CO^{18}O concentrations in the model. The δ notation, leading to isofluxes, discriminations etc. and used to display the results, is only introduced through post-processing. This guarantees mass conservation in our calculations.

2.3.1. Respiration

[16] From the above it follows directly the soil CO^{18}O flux, $^{18}F_R$:

$$^{18}F_R = \alpha_s R_s F_R = \alpha_s \alpha_{eq}(T_s)R_s^W F_R \qquad (11)$$

where R_s^W is the isotopic ratio of the soil water reservoir that exchanges with CO$_2$ and is taken directly from the water isotope module, and F_R is the CO$_2$ flux from the soil to the atmosphere which comes from BETHY (see below). Soil fractionation, $\epsilon_s = \alpha_s - 1$, is due to the different diffusivities of CO$_2$ and CO^{18}O in air. The maximum theoretical value is -8.7‰ is for a pure molecular diffusive process. The diffusion through the laminar-viscose boundary layer at the soil-atmosphere interface fractionates differently (approximately -5.8‰) and the effective diffusion fractionation depends on the relative influence of molecular and 'laminar-viscose' diffusion. Former studies of δ^{18}O-CO$_2$ [*Ciais et al.*, 1997a, 1997b; *Peylin et al.*, 1997, 1999] claimed that model outcome is sensitive to this parameter. Ciais et al. used a value of -5.0‰ in order to prevent a secular trend in δ^{18}O-CO$_2$ of the atmosphere. *Peylin et al.* [1997] studied the sensitivity of this fractionation factor together with the

fractionation associated with assimilation, and found possible values also around −5.0‰, matching the seasonal amplitude at Point Barrow and the inter-hemispheric difference. However, in their model $\delta^{18}O$ of atmospheric CO_2, δ_a, was forced to 0‰ versus VPDB-CO_2 and they used the fractionation factors of soil and above-ground vegetation as free parameters to obtain zero trend in their recalculated δ_a values. The ECHAM/BETHY isotope module calculates δ_a (R_a) and $CO^{18}O$ fluxes depending on δ_a (R_a) at every time step, and therefore δ_a stabilizes globally (see equation (23)). That means that the fractionation factors can theoretically have any possible value and δ_a will have no trend after the asymptotic equilibrium value is reached. For ϵ_s, we take the recent value of *Miller et al.* [1999]: $\epsilon_s = -7.2‰$. Miller et al. give this value for the fractionation of CO_2 diffusion from soils when one takes the soil water isotopic composition at 15 cm depth. They included in this global estimate the "invasion" effect that is explained below. We include the portion of the autotrophic respiration, F_{Rauto}, which is not emitted via leaves, $F_{Rroot} = F_{Rauto} - F_{Rleaf}$, into F_R. Most of the CO_2 of the autotrophic respiration F_{Rauto} is emitted by roots belowground (root respiration) and is thus subject to the same fractionation as the heterotrophic respiration. There is a small part of F_{Rroot} which is emitted aboveground by stems and twigs. *Bariac et al.* [1994a, 1994b] showed that there is almost no difference between the isotopic value of soil and plant organic water (except for leaves). Also, CO_2 in stems and twigs is expected to be in isotopic equilibrium with water. Thence we include this flux in F_{Rauto} so that F_R is the heterotrophic plus autotrophic (without leaf) respiration: $F_R = F_{Rhet} + F_{Rauto} - F_{Rleaf}$, which we call bio-respiration.

[17] There is another flux at the air-soil interface which exists for $CO^{18}O$ and not for CO_2. The transport of CO_2 is a diffusional process, and therefore the sum of two gross fluxes in and out of the soil. The flux into the soil is small because of the large mixing ratio difference of CO_2 in the soil and in the atmosphere. *Tans* [1998] wrote the net flux for $CO^{18}O$ as the sum of one flux leaving the soil, the above F_R, and a second flux of CO_2-molecules entering the soil with the atmospheric isotope signature, equilibrating with soil water and leaving the soil with the signature of soil water. This second flux is called the "abiotic flux" [*Stern et al.*, 2001] or "invasion flux" and the effect is called "invasion" [*Tans*, 1998]. This means, CO_2 with the isotopic composition R_a entering the soil equilibrates with soil water, R_s^W, and leaves the soil with the isotopic signature R_s. The invasion flux, $^{18}F_{inv}$, is then:

$$^{18}F_{inv} = \sqrt{\Theta_a \kappa \Theta_w^{18}k_H D_{18} B} c_a(R_s - R_a)$$
$$= F_{inv}(R_s - R_a) \qquad (12)$$

with
- Θ_a air-filled pore fraction of soil;
- κ tortuosity;
- Θ_w water-filled pore fraction;
- $^{18}k_H$ $CO^{18}O$ equilibration rate with $H_2^{18}O$, equal to $k_H/3$;
- D_{18} free-air molecular diffusivity of $CO^{18}O$;
- B Bunsen solubility coefficient.

F_{inv} may be seen as a virtual CO_2 flux, which is convenient for further calculations.

2.3.2. Assimilation

[18] CO_2 needs approximately 3 min at 10°C for hydration in water. The average residence time of a CO_2 molecule in the stomata is about 0.02 s [*Ciais et al.*, 1997a]. However, there is the enzyme carbonic anhydrase in leaves which catalyzes and speeds up the reaction by a factor of 10^7 [*Stryer*, 1981]. This implies that every CO_2 molecule entering the stomata is hydrated. Then, the isotopic equilibrium reaction (equation (7)) can take place and CO_2 is in isotopic equilibrium with the water between the mesophyll cell wall and the chloroplast. There is a gradient between the CO_2 concentration in the stomata, c_i, and in the chloroplast, c_c, during photosynthesis. There is no gradient if there is no photosynthetic activity. Leaf-scale measurements indicate that the average drawdown is of the order $(c_i - c_c)/c_a \approx 0.1 - 0.2$ [*Yakir and Sternberg*, 2000; *Lloyd and Farquhar*, 1994]. However, the equilibration process occurs mainly at the chloroplast or cellular membrane (plasmalemma) where the average drawdown is approximately 0.1 [*Gillon and Yakir*, 2000a]. We denote the mixing ratio where the equilibrium reaction occurs as c_{cs} because it is likely to be at the surface of the chloroplast [*Yakir*, 1998]. We take for c_{cs} the stomata-internal CO_2 mixing ratio c_i as a first guess and try to quantify the consequences of different equilibration places afterward (see the companion paper [*Cuntz et al.*, 2003]). Using c_{cs}, equation (1) becomes:

$$F_A = g_s(c_a - c_i) = g_s'(c_a - c_{cs}) \qquad (13)$$

where g_s' is the (harmonic) sum of the stomatal conductance and the conductance between the stomata and the plasmalemma (precisely the inverse of the sum of the resistances). Assuming that the conductance is very similar for CO_2 and for $CO^{18}O$, the diffusion equation (13) for $CO^{18}O$ is:

$$^{18}F_A = \alpha_l g_s'(R_a c_a - R_l c_{cs}) = \alpha_l g_s'(R_a c_a - \alpha_{eq}(T_v)R_l^W c_{cs}) \quad (14)$$

where $^{18}F_A$ is the flux of $CO^{18}O$ molecules into the leaves, α_l the kinetic fractionation factor for diffusion into the stomata ($\epsilon_l = -7.4‰$ [*Farquhar et al.*, 1993]), and R_l^W the isotopic composition of leaf water at the site of equilibration. Equation (13) shows that net assimilation is the sum of two opposing fluxes, in and out of the stomata. Rewriting the equation gives that the gross flux into the stomata is $F_A c_a/(c_a - c_{cs})$ and the flux out of the stomata is $F_A c_{cs}/(c_a - c_{cs})$. This means that only about 1/2 to 1/3 $[(c_a - c_{cs})/c_a]$ of all CO_2 molecules entering the leaf will finally be assimilated. The isotopic composition of leaf water at the site of equilibration, R_l^W, is calculated with the *Craig and Gordon* [1965] steady state approximation:

$$R_{l-cg}^W = \alpha_{l-vap}^W \left(\frac{(1-h)R_i^W}{\alpha_k^W} + hR_{vap}^W \right) \qquad (15)$$

with
- h relative humidity adjusted to leaf temperature;
- α_{l-vap}^W fractionation factor for $H_2^{18}O$ at the water-vapor phase transition;

α_k^W combined kinetic fractionation factor for H$_2$^{18}O for diffusion through the stomata and the leaf boundary layer;

R_{vap}^W ^{18}O/^{16}O ratio of water vapor in canopy air;

R_i^W ^{18}O/^{16}O ratio of xylem water, supplied to the leaf, approximately equal to ^{18}O/^{16}O ratio of soil water.

The isotope ratios of vapor and soil water are calculated from the water isotope module at every time step. Relative humidity is an ECHAM diagnostic variable (adjusted to leaf temperature), and the canopy is approximated by the first ECHAM model layer. The fractionation of the water-vapor phase transition is calculated from *Majoube* [1971]. The kinetic fractionation, ϵ_k^W, is higher for molecular than for turbulent diffusion [*Merlivat and Jouzel*, 1979]. It depends also on plant physiology [*White*, 1983] and on wind speed [*Förstel et al.*, 1975]. We take a global value of $\epsilon_k^W =$ −26.0‰ [*Farquhar et al.*, 1993] which itself results in an error. This error is diminished by the fact that α_k^W is weighted with the factor $(1-h)$ which is often close to 0. This is not true for dry areas but these are normally associated with low photosynthetic activity. The Craig and Gordon steady state approximation is probably not 'reached' by leaf water at every time step. Measurements indicate a time lag between measured values and values calculated with the Craig and Gordon model [e.g., *Roche*, 1999]. To overcome this problem, one can use a transitory model whereby the leaf water value is a mixture of the Craig and Gordon calculation and the value one time step before [*Dongmann et al.*, 1974; *Förstel et al.*, 1975; *Bariac et al.*, 1994a, 1994b]:

$$R_l^{W(t)} = R_{l-cg}^{W(t)} - \left(R_{l-cg}^{W(t)} - R_l^{W(t-1)} \right) \exp\left\{ -\frac{1}{\tau\zeta}\Delta t \right\} \quad (16)$$

with

$R_l^{W(t)}$ leaf water isotopic composition at the site of evaporation at time t;

$R_l^{W(t-1)}$ leaf water isotopic composition at time step $t-1$;

$R_{l-cg}^{W(t)}$ Craig and Gordon steady state solution at time t;

τ turnover time of leaf water, equal to V_l/E_v, where E_v is the transpiration rate and V_l is the leaf water volume;

ζ $=(1-h)(\epsilon_{l-vap}^W + 1)(\epsilon_k^W + 1)$.

To estimate the exponential weighting factor, one needs the leaf water volume contributing to evapotranspiration, V_l, for which, to our knowledge, there are no estimates in the literature for different plant functional types. So we compared the steady state Craig and Gordon model and the transitional nonsteady state model to laboratory measurements on Rajmah red kidney beans (*Phasedus vulgaris*) [*Roche*, 1999] and field measurements made during the EUROSIBERIAN CARBONFLUX (compare Appendix A) campaign in a 150 year old *Picea abies* (Norway Spruce) forest in Russia [*Langendörfer et al.*, 2002]. Both data showed a time lag of about two hours between Craig and Gordon and the transitory model and the transitory model compared much better with the measurements (results not shown here). Therefore we assigned τ a fixed value of about three hours (2/ln 2) to account for nonsteady state dynamic evolution of leaf water. This leads to a delayed development

of leaf water isotopic composition compared to Craig and Gordon. This implicates that the maximum leaf water enrichment is later in the day and also that night-time values of leaf water are much higher than calculated with Craig and Gordon. The transitional nonsteady state model imitates therefore the numerical solution of the isotopic diffusion equation in leaves [see *Cernusak et al.*, 2002].

[19] The enzyme carbonic anhydrase is distributed uniformly in the mesophyll cells and speeds up hydration of CO$_2$ in leaf water by a factor of 10^7 [*Stryer*, 1981]. This leads to the assumption that every CO$_2$ molecule once entered the stomatal cavity is almost instantaneously hydrated and soon isotopically equilibrated with leaf water. CO$_2$ molecules which cannot be carboxylated in plants because of limitations like electron transport, diffuse back in the atmosphere carrying the leaf water isotopic composition. Recent findings suggest that the carbonic anhydrase activity could be reduced so that not every CO$_2$ molecule which diffuses in the stomate becomes hydrated immediately but that a fraction of the CO$_2$ molecules could diffuse back in the atmosphere without being "tagged" by leaf water [*Gillon and Yakir*, 2000b, 2001]. This translates in equation (14) to a modified R_l. Let θ be the degree of equilibration expressed as a fraction, i.e., if 80% of all CO$_2$ molecules entering the leaf become hydrated immediately, $\theta = 0.8$. The fraction θ of the CO$_2$ molecules will still get the isotopic signature of leaf water where the remaining $(1-\theta)$ will only be affected by diffusion fractionation, α_l. The modified R_l, named R_{l-ca}, will then be [*Gillon and Yakir*, 2000b]:

$$R_{l-ca} = \theta R_l + (1-\theta)\left\{ 1 + \left(1 - \frac{c_{cs}}{c_a} \right)\alpha_l \right\}R_a. \quad (17)$$

The CO^{18}O flux is therefore equation (14) with R_l replaced by R_{l-ca}:

$$
\begin{aligned}
^{18}F_{A-ca} &= \alpha_l g_s'(R_a c_a - R_{l-ca}c_{cs}) \\
&= \alpha_l g_s'\left\{ R_a c_a - c_{cs}\left[\theta R_l + (1-\theta)\left\{ 1 + \left(1 - \frac{c_{cs}}{c_a} \right)\alpha_l \right\}R_a \right] \right\} \\
&= \alpha_l g_s'(R_a c_a - R_l c_{cs}) \\
&\quad - \alpha_l g_s'\left\{ (1-\theta)c_{cs}\left[\left\{ 1 + \left(1 - \frac{c_{cs}}{c_a} \right)\alpha_l \right\}R_a - R_l \right] \right\}. \quad (18)
\end{aligned}
$$

One can see that the second term in the difference is always positive (because the ratio of R_a will be only a few per mil lower than R_l, but R_a is multiplied by a factor between 1 and 2). The first term in the summation is the CO^{18}O flux with full carbonic anhydrase activity and it is normally positive. So the reduced carbonic anhydrase activity results in a reduced CO^{18}O flux from the atmosphere into the leaf. Measurements of *Gillon and Yakir* [2001] indicate that carbonic anhydrase activity is more reduced in C$_4$ plants than in C$_3$ plants. C$_4$ grasses for example can have a reduced carbonic anhydrase activity of down to $\theta = 0.4$ whereas C$_3$ plants lie around $\theta = 0.9$ or higher. Gillon and Yakir estimate a global mean θ of 0.78 with their vegetation distribution, and quite similar to our

global mean value of 0.8 with BETHY's vegetation distribution.

2.3.3. Ocean and Anthropogenic Emissions

[20] The CO^{18}O flux of the ocean is calculated as:

$$^{18}F_o = -\alpha_w R_a F_{ao} + \alpha_w R_o F_{oa}$$
$$= \alpha_w R_a F_o + \alpha_w(R_o - R_a)F_{oa} \qquad (19)$$

with

α_w	fractionation factor of CO$_2$ crossing the air-sea interface, including hydration;
R_a	^{18}O/^{16}O ratio of CO$_2$ in air;
R_o	^{18}O/^{16}O ratio of CO$_2$ equilibrated with ocean surface water;
F_{ao} and F_{oa}	CO$_2$ one way fluxes between atmosphere and ocean and vice versa;
F_o	net air-sea flux of CO$_2$ between atmosphere and ocean, equal to $F_{oa} - F_{ao}$.

The fractionation is taken as $\epsilon_w = +0.8‰$ [*Vogel et al.*, 1970]. The equilibration process is calculated via equation (8) with ECHAM driving climatological sea surface temperatures, and the ^{18}O/^{16}O of ocean surface water is fitted to the empirical relationship:

$$\delta_o^W = a_1 + a_2 \cdot SAL \qquad (20)$$

where *SAL* is the salinity in gram salt per kilogram water, and $a_1 = -16.75‰$ versus VSMOW and $a_2 = 0.5‰$ versus VSMOW are taken from *Ciais et al.* [1997a].

[21] Fossil fuel emissions and biomass burning are assumed to be without fractionation, i.e., that the CO$_2$ emitted carries the signature of atmospheric oxygen, R_f:

$$^{18}F_{fos} = R_f F_{fos} \qquad (21)$$

$$^{18}F_{bur} = R_f F_{bur} \qquad (22)$$

with $\delta_f = (R_f/R_{VPDB} - 1) \cdot 1000 = -17‰$ versus VPDB-CO$_2$; F_{fos} and F_{bur} are described in section 2.2.

2.3.4. Global Budget of δ^{18}O-CO$_2$

[22] One can write down the global budget equation for the temporal evolution of δ^{18}O in atmospheric CO$_2$ (taking only the processes of *Ciais et al.* [1997a, 1997b] for the moment):

$$\frac{d\delta_a}{dt} = \frac{1}{C_a M_a}\left[F_R \Delta_R + F_A \Delta_A + F_{ao} \Delta_o^{des}\right.$$
$$\left. + F_o \Delta_o^{equ} + (F_{fos} + F_{bur})\Delta_f\right] \qquad (23)$$

with

$$\Delta_R = \delta_s - \delta_a + \epsilon_s;$$
$$\Delta_A = -\epsilon_l + \frac{c_{cs}}{c_a - c_{cs}}(\delta_l - \delta_a);$$
$$\Delta_o^{equ} = \epsilon_w;$$
$$\Delta_o^{des} = \delta_o - \delta_a;$$
$$\Delta_f = \delta_f - \delta_a.$$

M_a is the conversion factor between fluxes in GtC and mixing ratios in ppm ($M_a = 2.122$ GtC ppm^{-1}, i. e., about 2 GtC are required to change the atmospheric CO$_2$ mixing

ratio by 1 ppm), Δ_A the discrimination of photosynthesis, and Δ_o^{equ} the equilibrium discrimination between ocean and atmosphere. The others are not real discriminations in a proper physical sense but follow the same mathematical description [*Farquhar et al.*, 1982]. These Δs are simply the difference between the δ-value of the CO$_2$ flux and the atmospheric δ-value, δ_a. We use the same symbol, Δ, for simplicity and denote them in this paper generically "apparent discriminations". Δ_R is therefore the apparent discrimination associated with soil-respired CO$_2$, Δ_o^{des} the ocean disequilibrium or the tendency to equilibrate the difference between atmospheric and ocean dissolved CO$_2$, and Δ_f the difference between the isotopic signature of O$_2$ (involved in combustion) and CO$_2$. Analogous to plain CO$_2$, one calls the product of CO$_2$ flux and apparent discrimination an isoflux. Just as the change of CO$_2$ in the atmosphere is the sum of all CO$_2$ fluxes, the change of δ^{18}O is the sum of all isofluxes. One can rewrite equation (23) as a differential equation:

$$\frac{d\delta_a}{dt} = k_1 - k_2 \delta_a \qquad (24)$$

whose solution is an exponential evolution of atmospheric δ^{18}O-CO$_2$ with time:

$$\delta_a(t) = \frac{k_1}{k_2} + \left(\delta_{a0} - \frac{k_1}{k_2}\right)\exp\{-k_2 t\}. \qquad (25)$$

The factor k_1 is a combination of CO$_2$ fluxes and δ-values in the compartments, and k_2 consists only of positive CO$_2$ fluxes, by definition. δ_{a0} is the (arbitrary) value of the atmosphere at time $t = 0$. Therefore this is a stable differential equation, and the global δ^{18}O value stabilizes at k_1/k_2 when t becomes infinite:

$$k_1 = \frac{1}{C_a M_a}\left[F_R(\delta_s + \epsilon_s) + F_A\left(\epsilon_l + \frac{c_{cs}}{c_a - c_{cs}}\delta_l\right) + F_{ao}\delta_o\right.$$
$$\left. + F_o \epsilon_w + (F_{fos} + F_{bur})\delta_f\right] \qquad (26)$$

$$k_2 = \frac{1}{C_a M_a}\left[F_R + \frac{c_{cs}}{c_a - c_{cs}}F_A + F_{ao} + F_{fos} + F_{bur}\right]. \qquad (27)$$

In contrast to earlier simulations of δ^{18}O in atmospheric CO$_2$, we do not have to adjust the fractionation factors to obtain a stable solution. We rather calculate δ_a at every time step and couple it to the CO^{18}O surface fluxes, and hence δ_a will always stabilize if there is no trend in the CO$_2$ fluxes or the δ-values in the compartments, e.g., the water isotopic composition.

[23] Including other processes in the calculation of δ^{18}O just adds fluxes and/or isofluxes in the global budget equation. Invasion for example adds the isoflux $F_{inv}\Delta_{inv}$ to equation (23) with $\Delta_{inv} = \delta_s - \delta_a$, the apparent discrimination of invasion. This in turn adds terms within the parentheses of equations 26 and 27, which adds $F_{inv}\delta_s$ to the parenthesis of k_1, and F_{inv} to the parenthesis of k_2, for the invasion effect. This changes the global mean value that δ_a approaches with time, k_1/k_2. The effect of invasion now

reduces the global mean δ_a. The proposed reduced activity of carbonic anhydrase changes leaf discrimination to:

$$\Delta_{A-ca} = -\epsilon_l + \frac{c_{cs}}{c_a - c_{cs}}\left\{\theta(\delta_l - \delta_a) + (1 - \theta)\left(1 - \frac{c_{cs}}{c_a}\right)\epsilon_l\right\}$$

$$= -\epsilon_l + \frac{c_{cs}}{c_a - c_{cs}}(\delta_l - \delta_a)$$

$$- \frac{c_{cs}}{c_a - c_{cs}}(1 - \theta)\left\{\delta_l - \delta_a - \left(1 - \frac{c_{cs}}{c_a}\right)\epsilon_l\right\}. \quad (28)$$

The first two terms are leaf discrimination with full carbonic anhydrase activity, Δ_A, so that a reduced carbonic anhydrase activity normally reduces leaf discrimination and the global mean δ_a value will also stabilize at a lower value.

3. Results

[24] In order to validate our model, we have to validate first the different modules: the biosphere model and associated CO_2 fluxes, the $CO^{18}O$ fluxes, the water isotope ratios, and the atmospheric transport. We focus in this paper on the surface processes and compare the outcome of our model with other estimates and observations. We will validate only the terrestrial biosphere component and exclude ocean fluxes, fossil fuel and biomass burning. We show in part 2 that in order to simulate the seasonal cycle at almost all stations and to simulate the north-south gradient, ocean fluxes, fossil fuel, and biomass burning are not essential; contrary to the results of *Ciais et al.* [1997a, 1997b]. For the north-south gradient, this comes mainly from the fact that in our model, the atmospheric $\delta^{18}O$-CO_2 mixing ratios influence the $\delta^{18}O$ fluxes. This was not implemented in prior $\delta^{18}O$-CO_2 models. BETHY offline was validated extensively by *Knorr* [1997, 2000] and *Knorr and Heimann* [2001a, 2001b] but the implementation of BETHY in ECHAM can lead to very different results. ECHAM/BETHY computes for example on a much coarser grid than BETHY offline and the meteorological parameters are taken from ECHAM which is of course different than the climatologies of *Leemans and Cramer* [1991] used in BETHY offline. One example of differing results is the global annual NPP which amounts to 70.0 GtC yr^{-1} in BETHY offline and 55.7 GtC yr^{-1} in BETHY online.

3.1. Fluxes and Apparent Discriminations

[25] The sum of all CO_2 fluxes determines the temporal change of the CO_2 mixing ratio in the atmosphere; the sum of the isofluxes of $\delta^{18}O$-CO_2 determines the change of $\delta^{18}O$ in atmospheric CO_2, accordingly. We calculate CO_2 fluxes and isofluxes directly in our model, so the apparent discriminations are a combination of both, namely, the ratio of isoflux and CO_2 flux. Our back-calculated apparent discriminations are consequently flux-weighted discriminations. Earlier $\delta^{18}O$-CO_2 models calculated CO_2 fluxes and discriminations separately and multiplied them to get isofluxes. These apparent discriminations were thus not flux-weighted. They tried to get around this problem using flux-weighted variables to calculate their discriminations, therebyneglecting nonlinearities in the calculations, mainly in the discrimination associated with assimilation. Inconsistencies among the different models, used to calculate isofluxes in the end,

Table 2. Global Annual CO_2 Fluxes, Assimilation Weighted Annual Mean CO_2 Mixing Ratios, Assimilation Weighted Annual Mean δ Values, and ϵ Constants Calculated and Used in ECHAM/BETHY[a]

Flux, Mixing Ratio, δ, ϵ/	Value in ECHAM/BETHY
F_A	97.3
F_R	98.0
F_{ao}	99.4
F_o	2.6
F_{fos}	5.8
F_{bur}	3.1
c_a	353
c_{cs}	264
δ_l	6.3
δ_s	−6.9
δ_o	1.2
δ_f	−17.0
ϵ_l	−7.4
ϵ_s	−7.2
ϵ_w	0.8

[a]Global annual CO_2 fluxes are given in GtC yr^{-1}, assimilation weighted annual mean CO_2 mixing ratios are given in ppm, assimilation weighted annual mean δ values are given in ‰ versus VPDB-CO_2, and ϵ constants are given in ‰.

added errors which were neither commensurable nor estimable. This problem is not present in our model, in which CO_2 fluxes and isofluxes are consistently calculated, leading to apparent discriminations that can be compared to measurements. Unfortunately, measurements of discriminations of $\delta^{18}O$-CO_2 are difficult to achieve and therefore very sparse in the literature.

[26] Table 2 gives an overview of the main variables calculated and used in ECHAM/BETHY. The table includes all necessary values to calculate the global budget and/or the asymptotic global δ_a value. F_A is thereby not GPP but net assimilation that is GPP minus leaf respiration. F_R is therefore what we call biorespiration that is heterotrophic plus autotrophic minus leaf respiration. The δ values are consequently flux-weighted means, weighted with the fluxes on every time step of 40 minutes. It is noteworthy that δ_l, the isotopic composition of CO_2 equilibrated with leaf water at the evaporating site, is about 2‰ higher than former estimates, like, e.g., *Ciais et al.* [1997a]: $\delta_l = 3.9‰$ versus VPDB-CO_2.

[27] Figure 2 shows seasonal cycles of the sum of CO_2 fluxes and isofluxes in 30° latitude bands, and resulting apparent discriminations as 30° zonal means. CO_2 fluxes are given in GtC month^{-1} so one can see that the northern boreal zone (30° to 60°N) is even more productive during the northern summer than the tropical zone during austral summer. Poleward of 60°N, net assimilation (and biorespiration) decreases visibly. The seasonal cycle of leaf discrimination seems to contradict intuition but one can see in the apparent soil discrimination that soil water isotopes do not change significantly during the course of a year (we examine this further in the section about the nighttime terrestrial source signature). It is therefore increasing leaf temperature during summer together with decreasing c_i values which dominate the leaf discrimination signal and lead to lower discrimination during summer compared to winter. Contrary to assimilation, the northern boreal zone does not show the same maximum value in leaf isoflux as
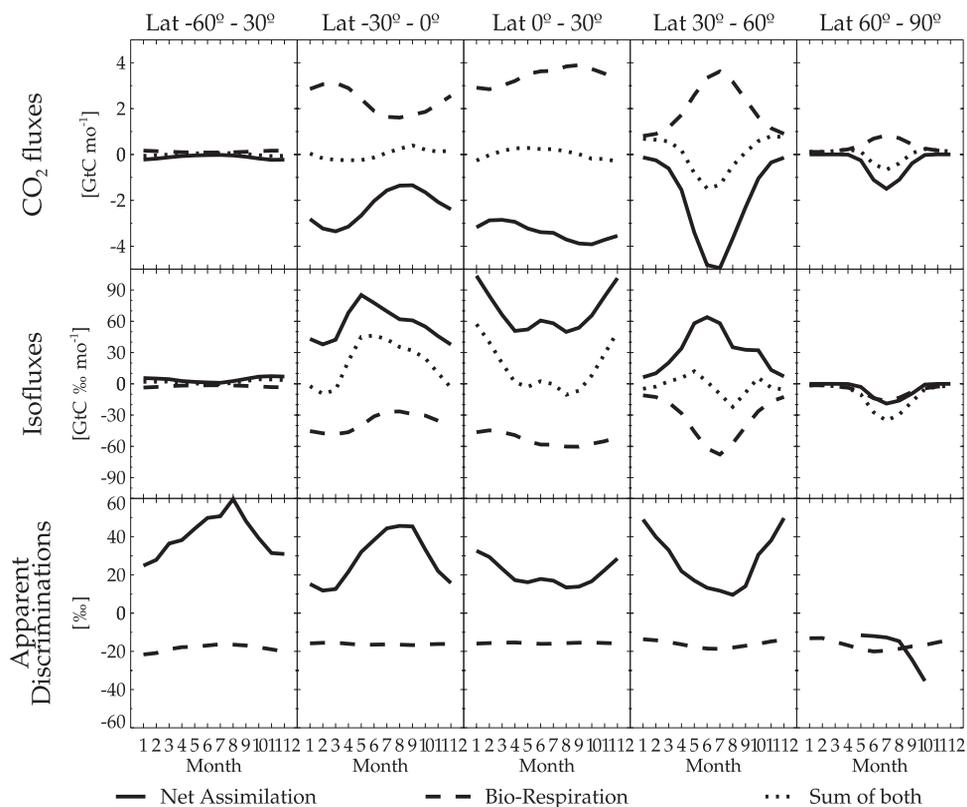
Figure 2. Seasonal cycle of the sum of CO_2 fluxes and isofluxes, and resulting apparent discriminations (isoflux/CO_2 flux) in 30° latitude bands calculated by ECHAM/BETHY. Here, mo, month.

the tropical zone does. Comparing 30° to 60°N with 0° to 30°S shows that leaf discrimination diminishes similarly during the respective summer with about 40‰ in winter and 20‰ in summer. However, winter CO_2 assimilation is much higher in the southern latitude band, which, along with high discriminations, leads to the peak in leaf isoflux in the southern winter. Leaf discrimination becomes negative in high northern latitudes (missing values come from numerical instabilities at very low net assimilation when postprocessing). In Eurasia, 25% of the cause of negative leaf discrimination can be attributed to the depletion of rain in the interior of the continent and 75% can be attributed to the increase of relative humidity from West to East Siberia which biases leaf water at the evaporating site to the isotopic composition of water vapor rather than to soil water [*Cuntz et al.*, 2002]. ECHAM temperatures are about 2°C lower than those from ECMWF re-analysis in East-Siberia but very similar to ECMWF in Canada and Alaska [*Roeckner et al.*, 1996]. Lower temperature translates into higher relative humidities which in turn gives lower leaf water values and consequently lower leaf discriminations (2°C lower temperature translates to about 10‰ lower leaf discrimination in our model). The ECMWF re-analysis in Eastern-Siberia is very questionable because it is not well constrained, because of sparse measurement coverage. We think that it is realistic that leaf discrimination should become negative in Eastern-Siberia, and it should be measurable, as argued by *Cuntz et al.* [2002]. Negative photosynthetic discrimination is in fact directly implied by some concurrent vertical profiles of CO_2 and $\delta^{18}O$-CO_2 in and

above the convective boundary layer for central Siberia, even in mid-summer [*Lloyd et al.*, 2002a; *Styles et al.*, 2002a]. We show in Figure 3a the assimilation-weighted annual mean leaf discrimination (in ‰), which can be compared to other estimates (e.g., to *Farquhar et al.* [1993]). One can see that leaf discrimination becomes negative already at around 45°N in certain regions. On the other hand, Australia, Africa, and South America are very uniform in their mean discrimination (except for the Andes). The distribution pattern of leaf discrimination is similar to the one estimated by *Farquhar et al.* [1993] but differs in magnitude by approximately a factor of 2. Farquhar et al. calculate a global mean leaf water isotopic composition of 4.4‰ versus VSMOW, weighted by assimilation on a monthly basis, whereas our leaf water isotopic composition is 6.3‰ versus VSMOW, weighted by assimilation on every time step of 40 minutes. Farquhar et al. have a global mean stomata-internal CO_2 mixing ratio, c_i, of 235 ppm while we calculate a mean of 264 ppm. They do not take c_i but the CO_2 mixing ratio at the chloroplast, c_c, which further reduces their enhancement factor $c_{cs}/(c_a - c_{cs})$ (where c_{cs} is either c_i or c_c) to about 1.3 in the global mean, compared to about 3 in our model. Taking assimilation-weighted leaf water isotopic composition on a sub-daily basis is certainly more realistic but whether c_{cs} is closer to c_i or c_c is still a matter of debate (see below).

[28] Unlike leaf discrimination, the apparent soil discrimination is not real discrimination. What we call apparent discrimination is the difference between the isotopic signature of the CO_2 flux of one process and the $\delta^{18}O$-CO_2 in the
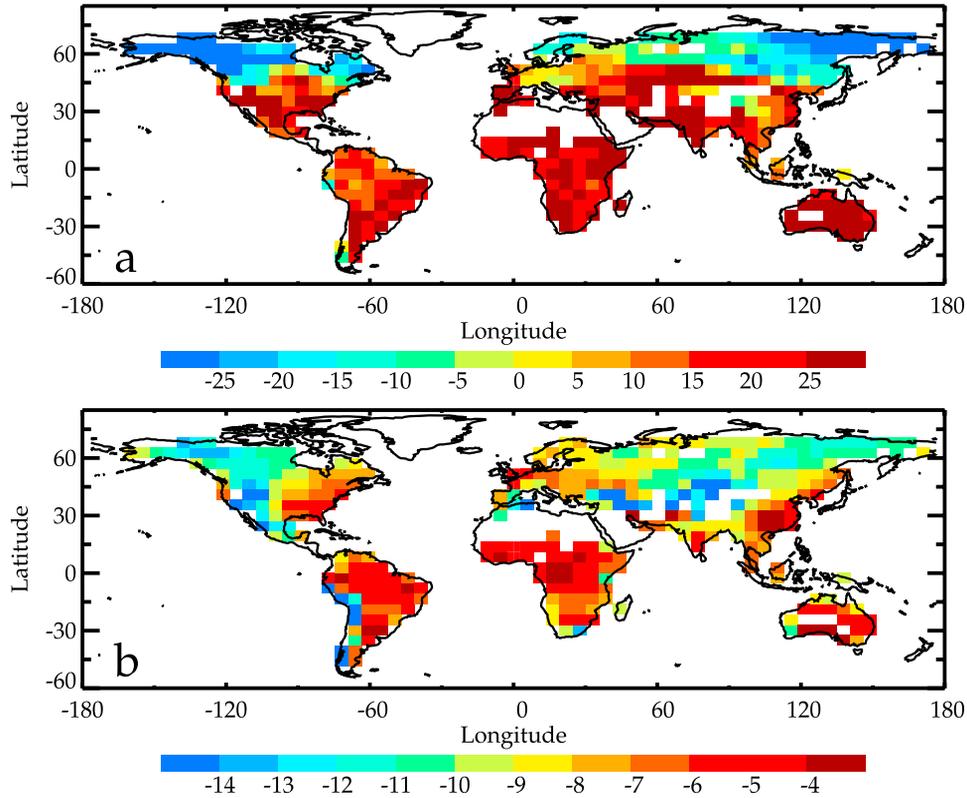
Figure 3. (a) Annual mean leaf discrimination in ‰ and (b) annual mean isotopic composition of CO₂ in equilibrium with soil water in ‰ versus VPDB-CO₂, calculated by ECHAM/BETHY.

atmosphere. While the isotopic signature of the CO₂ soil flux does not depend on the atmospheric δ¹⁸O level, apparent soil discrimination does. One can see in equation (11) and equation (14) that the CO¹⁸O flux of respiration is independent of the isotope ratio in the atmosphere, R_a, whereas the CO¹⁸O flux of assimilation depends on it. If we include a new process in our calculation (e.g., computing with or without fossil fuel fluxes), the atmospheric δ¹⁸O level will change, according to equations 23–27. This will change the apparent soil discrimination but the soil CO¹⁸O flux will stay the same. The leaf CO¹⁸O flux instead will adapt to the new δ¹⁸O level in the atmosphere so that leaf discrimination and apparent soil discrimination will change differently. (In contrast to ¹³C, δ_a does not cancel out in leaf discrimination of ¹⁸O.) We show in Figure 3b the isotopic composition of CO₂ equilibrated with soil water in ‰ versus VPDB-CO₂ (and not the apparent soil discrimination in ‰). To derive the apparent soil discrimination from Figure 3b, one has to add soil fractionation during diffusion, ϵ_s taken as -7.2‰ [*Miller et al.*, 1999] in the model, and subtract the atmospheric δ¹⁸O-CO₂. ¹⁸O isotopes in soil CO₂ are quite uniform inside continents and result in about -11‰ versus VPDB-CO₂ in the northern hemisphere and about -5 versus VPDB-CO₂ in the southern hemisphere. This result is very similar to *Ciais et al.* [1997a], which is surprising, because Ciais et al. used rain isotopic composition and we use soil isotopic composition, and the large seasonal cycle of isotopes in rain is very much attenuated. In addition, our annual values are all flux-weighted. We will show below that CO₂ leaving the soil in our model is isotopically almost constant during the year. Our respiration weighted

annual mean is therefore very similar to our unweighted annual mean. Because soil integrates the rain signal over long time periods, the annual mean of isotopes in rainwater and soil water are very similar. Thus we end up with an annual mean isotopic composition of CO₂ in equilibrium with soil water very similar to the estimate of *Ciais et al.* [1997a].

3.2. Net Primary Productivity

[29] The Potsdam NPP Model Intercomparison Project [*Kicklighter et al.*, 1999] compared 15 net primary productivity models. The shadowed area in Figure 4 shows the range between the 10th and 90th percentiles of the 15 models together with the median (grey solid line). Note that y axis units are in gC m⁻² s⁻¹. The BETHY online model (black solid line) is very similar to the median of the 15 models and lies well in between the 10th to 90th percentile range. The most noteworthy difference is the lower productivity of ECHAM/BETHY at high latitudes. In the northern hemisphere poleward of 60°N, ECHAM/BETHY is at the 10th percentile level of the intercomparison and in the southern hemisphere between 40° and 45°S, it falls even below the 10th percentile level. We included in Figure 4 (black dotted line) the gridded data set compiled by the Ecosystem Model-Data Intercomparison (EMDI) project [*Olson et al.*, 2001] (details in Appendix A). In the southern extra-tropics, the NPP measurements of EMDI are primarily from grassland. Grassland NPP measurements are often pointwise above-ground NPP measurements, converted to total NPP with a constant factor. EMDI used a conversion factor of 2 to calculate total NPP from pointwise measured
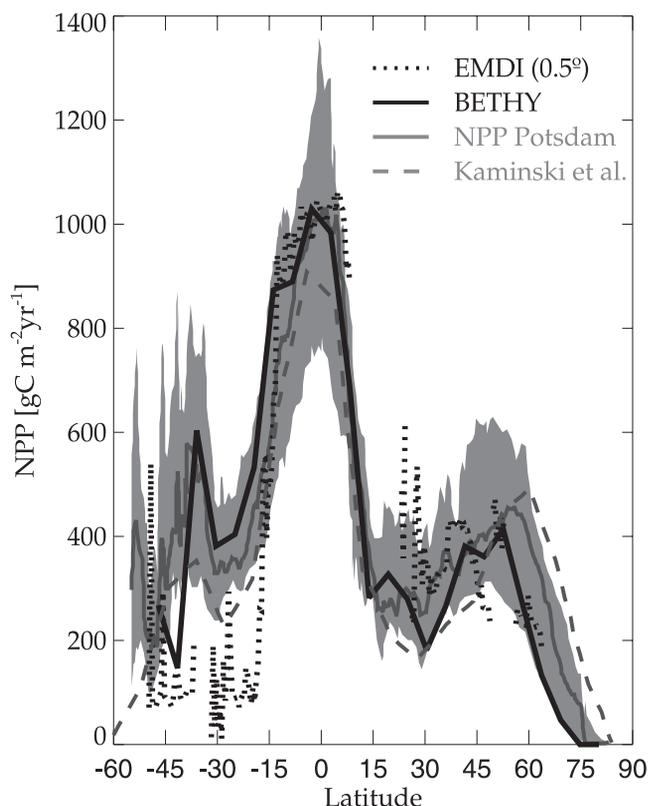
Figure 4. Comparison of Net Primary Productivity (NPP) of the EMDI measurement compilation (black dotted line), the Potsdam NPP model intercomparison [*Kicklighter et al.*, 1999] (grey solid line, plus area between 10th and 90th percentiles, grey), BETHY online (black solid line), and result of a data assimilation study [*Kaminski et al.*, 2002] (grey dashed line) as latitudinal average.

above-ground NPP. This factor seems to be too low for grasslands because grasses may lose carbon to processes which are hidden from single above-ground NPP measurements. For instance, the above-ground part of grasses can be eaten by herbivores, destroyed by fires or die because of environmental conditions and can regrow afterward, while the belowground part of the grasses can lose carbon because of exudates or secretions of roots, or transfer of carbon to mycorrhizae [*Long et al.*, 1989]. At any rate, the EMDI estimates are a factor of 4 lower than the model results. *Scurlock et al.* [2002] compared different methods of estimating NPP of grasslands and found differences of up to a factor of 3 in the NPP estimates of different methods. So it is not certain that our model values are too high, but they should be taken with care. On the rest of the globe, the median of the 15 models and BETHY online compare well with the NPP estimations. Poleward of 50°N, the NPP data seems to agree more closely with the lower range of the Potsdam NPP models, and especially ECHAM/BETHY. However, there are only few measurements in the data compilation poleward of 50°N, ending around 60°N, so that tundra vegetation is not represented whereby tundra vegetation has potentially the same conversion problems as grasslands. Also included in the Figure 4 is the result of a data assimilation study (grey dashed line) [*Kaminski et al.*, 2002] that will be discussed in section 4. It is noteworthy

that all estimates of global annual NPP, including the data compilation, lie all very close together around 55 GtC yr⁻¹ (see Table 3) whereby the models of the Potsdam NPP Model Intercomparison show a range of about 40 to 80 GtC yr⁻¹. *Knorr and Heimann* [2001b] optimized the BETHY offline model with satellite data and found that a global annual NPP of 70 ± 35 GtC yr⁻¹ is consistent with measurements of the CO_2 atmospheric seasonal cycle and with reflectance measurements from satellite. Sensitivity runs of BETHY offline showed a range of 48.3 − 77.1 GtC yr⁻¹ [*Knorr*, 2000] with the bulk of sensitivity runs yielding approximately 62 GtC yr⁻¹. The largest uncertainty comes thereby from the formulation of respiration and the second largest uncertainty from the used assimilation description. For example, using a light-use efficiency formulation [*Monteith*, 1977], NPP changes by about 13%. However, BETHY online simulates reasonable NPP with a conservative estimate of NPP over almost the whole latitude range except for the high northern latitudes where it predicts comparably low NPP values.

3.3. Net Ecosystem Exchange

[30] We now compare the CO_2 flux component of our model with eddy flux measurements of Net Ecosystem Exchange (NEE). Although our model has a grid dimension of about 500 km, while eddy flux measurements represent an area of around 1 km², this is nevertheless a useful semi-quantitative indication of the ECHAM/BETHY model performance. In addition, most NEE measurement sites are located in young regrowing forests which gives a bias toward higher absolute NEE values. Also, the climate for our NEE calculations is simulated by ECHAM and is thus not the one observed at the stations. However, the phasing of NEE in our model should be comparable to that of the measurements, and the amplitude should be of the same order of magnitude. We used the compilation of eddy flux measurements of FLUXNET [*Running et al.*, 1999] (FLUXNET data are available from the ORNL DAAC at http://www. daac.ornl.gov/) and added two forest sites in western and central Russia [*Milyukova et al.*, 2002; *Lloyd et al.*, 2002b; *Shibistova et al.*, 2002] (details in Appendix A). We chose only those stations for which we have the same ecosystem in the corresponding grid cell of the model (or surrounding grid cells). If the model does not have the same ecosystem in the appropriate grid cell, we took an adjacent grid cell if possible, otherwise discarded the station. A list of all 20 stations used, including the associated BETHY plant functional type number, can be found in Table A1.

[31] Figure 5 shows the comparison between BETHY online monthly mean NEE fluxes and individual measure-

Table 3. Global Annual Net Primary Productivity[a]

Model/Data Estimate	Global NPP, GtC yr⁻¹
ECHAM/BETHY	55.7
Potsdam Range	39.9−80.5
Potsdam Mean	55.4
Kaminski et al. [2002]	54.9
EMDI Data (Estimate)	∼55
BETHY offline	70.0

[a]The range and mean of the Potsdam NPP Intercomparison comes from *Cramer et al.* [1999], considering only the 15 models of *Kicklighter et al.* [1999]. The EMDI global estimate was calculated using a polynomial fit through the data of Figure 4.
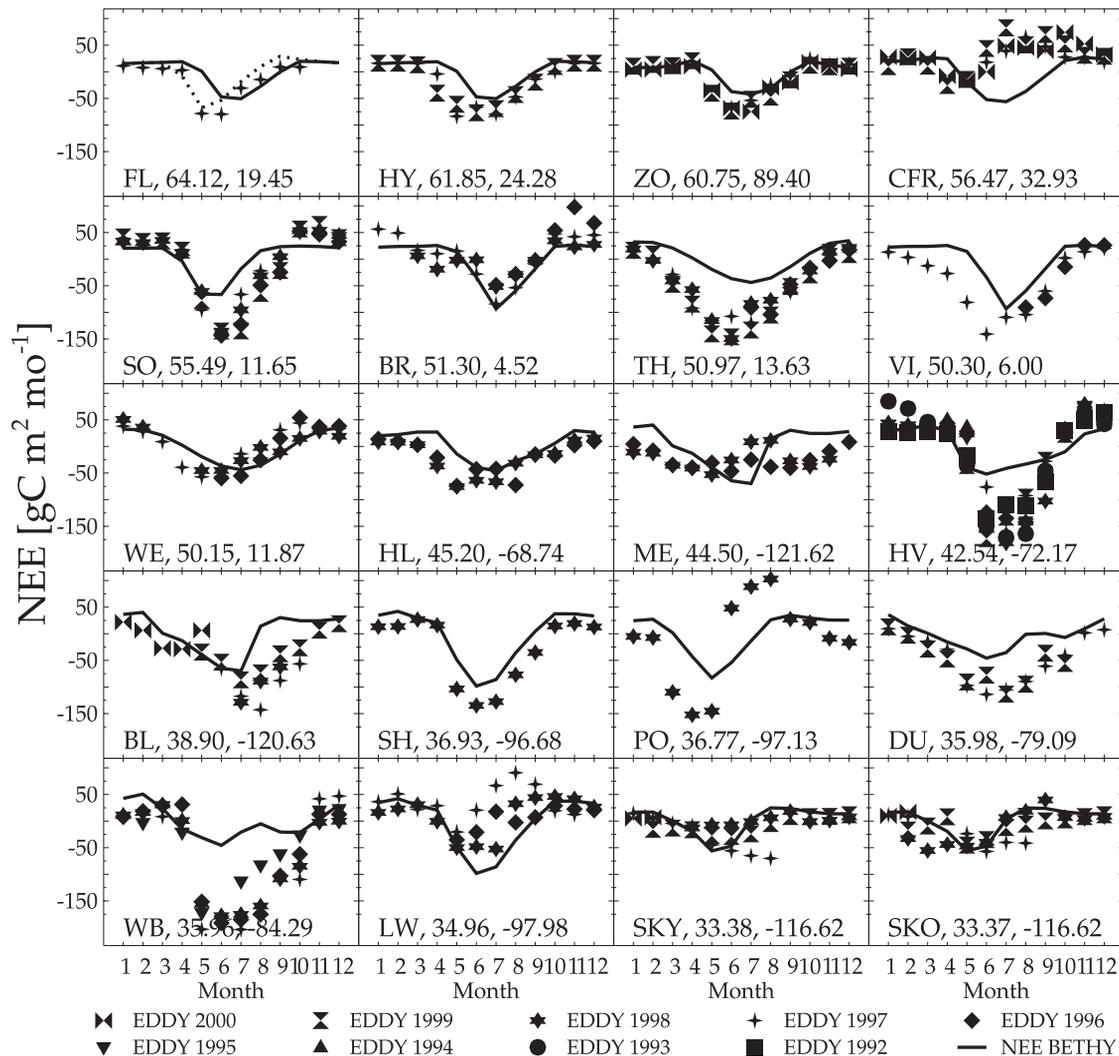
Figure 5. Net Ecosystem Exchange (NEE) at 20 different eddy flux sites (different symbols for each year) compared to mean ECHAM/BETHY (solid line). The values after the station abbreviation stand first for latitude and second for longitude of the site. The sites are in descending latitude order. The dotted line at Flakaliden is model NEE with assimilation shifted arbitrarily one month in advance.

ment years, the latter to demonstrate the large interannual variability of the measurements. ECHAM's monthly means variables, aggregated from 40 minute output, instead represent a climatological mean state, so there is no such interannual variability. We arranged the sites in latitudinal order so that one can easily see that all sites are poleward of 30°N and mainly in Europe and North America. ECHAM/BETHY seems to underestimate the NEE flux amplitude at half of the stations. Notably poleward of 60°N, ECHAM/BETHY is too low in amplitude which corresponds to the low NPP predictions of ECHAM/BETHY at high northern latitudes (compared to the 15 NPP models, not compared to the EMDI NPP data compilation). The model overpredicts minimum NEE only at Central Forest Reserve (CFR) and Little Washita (LW) which both show a source of CO$_2$ in the measurements (this is not possible in the model because NEE is set to zero in the long term mean). The limit of the comparison can be seen at the stations Braschaat (BR), Tharandt (TH), Vielsalm (VI), and Weidenbrunnen (WE) which all lie in close proximity. They

occupy actually only two neighboring grid cells in the model, so Braschaat and Vielsalm as well as Tharandt and Weidenbrunnen are compared to the same NEE flux of the model. However, one can see that the compared stations show a different NEE amplitude, about a factor of 2 larger. So ECHAM/BETHY simulates much better the lower NEE amplitude stations. In the latitude range poleward of 50°N, ECHAM/BETHY is always slightly out of phase. Its minimum NEE arrives about one month too late. This behavior cannot be seen between 30° and 40°N and the comparison is equivocal in between.

3.4. Stomata CO$_2$ Mixing Ratio

[32] The CO$_2$ mixing ratio inside stomates is an important variable for leaf discrimination (see equation (23)). The factor $c_{cs}/(c_a - c_{cs})$ amplifies the difference between leaf water equilibrated CO$_2$ and atmospheric δ^{18}O-CO$_2$. At an ambient CO$_2$ mixing ratio of 350 ppm and a stomatal CO$_2$ mixing ratio of 230 ppm, this factor is about 2. With further drawdown of c_{cs}, the factor diminishes as well, reaching 1 at
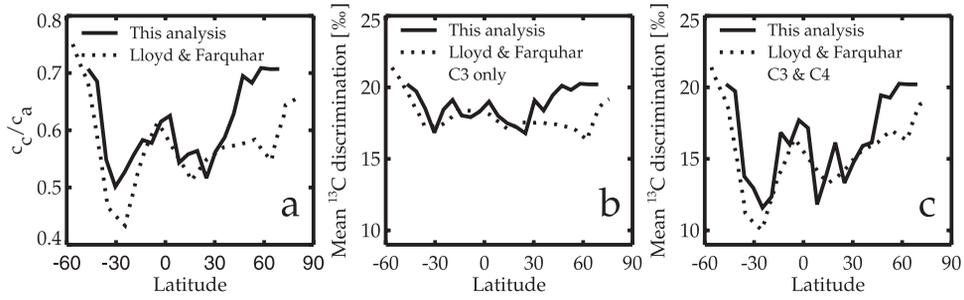
Figure 6. Latitudinal distribution of the stomata-internal CO_2 mixing ratio. The ratio of stomatal to atmospheric CO_2 mixing ratio is compared with *Lloyd and Farquhar* [1994] via c_c/c_a for (a) C_3 and C_4 plants, (b) ^{13}C photosynthetic discrimination of C_3 assimilation and (c) C_3 together with C_4 assimilation.

175 ppm. Even lower values of c_{cs}, e.g., at high assimilation rates, lead to a vanishing influence of leaf water on atmospheric $\delta^{18}O$-CO_2. We explained in section 2.3 that we take as a first guess the stomata-internal CO_2 mixing ratio c_i as an estimate of c_{cs}. Our global assimilation weighted value of c_i is very high with 264 ppm. This leads to $c_{cs}/(c_a - c_{cs}) = 3$. This comes from the fact that we start from rather high non-water-limited c_i values, which come from *Schulze et al.* [1994]. This literature survey of field measurements gives a c_{i0} of 0.87 c_a for C_3 plants which is much higher than laboratory measurements suggest: ∼0.7 c_a [*Farquhar et al.*, 1989b; *Boyer et al.*, 1997]. We try to validate our c_i estimates indirectly via ^{13}C leaf discrimination. However, ^{13}C fractionation by photosynthesis is determined by CO_2 mixing ratio in the chloroplast, c_c, rather than in the stomata. *Lloyd and Farquhar* [1994] give a range of 0.16 c_a to 0.2 c_a for the difference between c_i and c_c at saturating photon irradiance. They use a value of 0.1 c_a suggesting leaves operating on roughly 50% of their maximum (light-saturated) photosynthetic capacity. *Yakir and Sternberg* [2000] recommend a value of 0.2 c_a for an average drawdown on the chloroplast level. We take a value midway between the different estimates and $c_i - c_c = 0.16\,c_a$.

[33] In Figure 6a, the latitudinal distribution of c_c/c_a in ECHAM/BETHY is compared to the estimate of *Lloyd and Farquhar* [1994]. Both estimates are similar, but be aware that the global mean level of both curves depend on the above discussed drawdown from c_i to c_c. The difference in the southern hemisphere comes mainly from the different distribution of C_4 plants in the two approaches. This can also be seen comparing Figures 6b and 6c. We calculated, along with c_c/c_a, the ^{13}C leaf discrimination of C_3 plants, using the simple formula [*Farquhar et al.*, 1989a]:

$$\Delta_A^{13}C = a + (b - a)\frac{c_c}{c_a}. \qquad (29)$$

$a = 4.4‰$ is the kinetic fractionation of ^{13}C diffusion in air and b is the fractionation associated with carboxylation. There is a considerable amount of uncertainty regarding the correct value of b. *Farquhar et al.* [1989a] found the best fit to measurements with $b = 27‰$ but using c_i instead of c_c. *Lloyd and Farquhar* [1994] expanded the formula of Farquhar et al. by dividing the gradient between stomata and chloroplast into several components. b is therefore a mixture of carboxylation of RUBISCO (RibUlose BISpho-

sphate Carboxylase/Oxygenase) ($b_3 = 29‰$) and 5 to 10% carboxylation of PEP (phospho enolpyrvate) carboxylase ($b_4 = -5.6‰$ at 25°C). They found a value of $b = 27‰$ but using c_c. We follow their later conclusions and take $b = 27‰$ together with c_c for C_3 plants. We take a constant value of $a = 4.4‰$ for C_4 plants. Taking only the simple formula (equation (29)) for calculating $\Delta_A^{13}C$ is of minor importance because the expansion of Lloyd and Farquhar results in only small changes in the latitudinal mean compared to the simple formula. Note that we follow the historical convention that fractionation and therefore discrimination in ^{13}C and ^{18}O have opposite signs. So the isoflux of $\delta^{13}C$ is $-\Delta_A^{13}C$ times assimilation and the isoflux for $\delta^{18}O$ is $+\Delta_A^{18}O$ times assimilation, i.e., a positive $\Delta_A^{13}C$ is comparable in its effect on the atmosphere to a negative $\Delta_A^{18}O$. Plotted in Figure 6b is the latitudinal distribution of ^{13}C discrimination of C_3 plants only and in Figure 6c of C_3 and C_4 plants together. (Figures 6a and 6c are very similar and are different presentations of the same result. However, Figure 6a is the actual variable we are interested in, Figures 6b and 6c show the results detailed for C_3 and C_4 plants in a notation that is, via equation (30), closely related to Figure 7, the comparison with observations.) The C_3 distributions are extremely similar except for the high northern latitudes. Poleward of 30°N, the two estimates diverge. ECHAM/BETHY reaches its base, non-water-
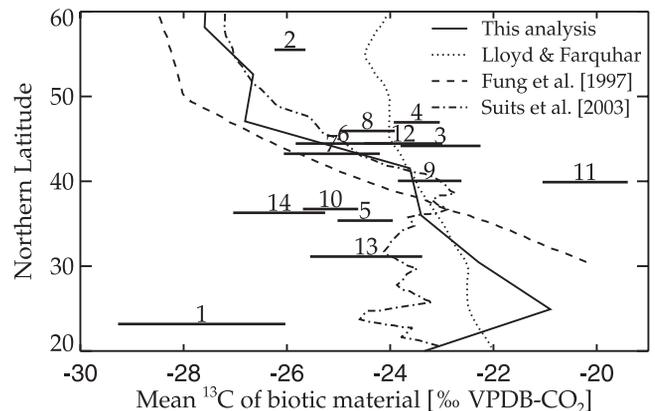
Figure 7. Latitudinal distribution of $\delta^{13}C$ source signature, $\delta_{bio}^{13}C$. Both studies of Figure 6 are compared to measurements of mean biotic ^{13}C of *Miller et al.* [2003]. The numbers correspond to continental sampling sites of NOAA/CMDL and are explained in Table A2.

limited level of c_c/c_a of about 0.71 (=0.87−0.16) (Figure 6a) whereas Lloyd and Farquhar do not reach such high values (they do in the southern extra-tropics). Lloyd and Farquhar remarked the same phenomena in comparison to earlier estimates of *Farquhar et al.* [1993] that also diverged at high northern latitudes. The differences between BETHY online and the earlier investigation below 30°N come mainly from the different distribution of C$_4$ plants. With the vegetation distribution used, big parts of the African vegetation belt are covered by C$_4$ long grasses, which give the modeled minimum Δ_A^{13}C at 10°N. C$_4$ plant assimilation contributes 21% of global GPP according to *Lloyd and Farquhar* [1994] whereas BETHY online calculates 18%; C$_4$ long grasses alone (PFT 12, Table 1) contribute 12%. This gives a mean discrimination for the terrestrial biosphere of 16.1‰ versus VPDB-CO$_2$ in BETHY online compared to 14.8‰ versus VPDB-CO$_2$ of Lloyd and Farquhar. For C$_3$ plants only, BETHY online gives 18.7‰ whereas Lloyd and Farquhar estimate 17.8‰ versus VPDB-CO$_2$. However, the overall global mean discrimination deviates quite a lot from other investigations: 15.7‰ [*Fung et al.*, 1997], 18.0‰ [*Tans et al.*, 1993], 20.0‰ [*Quay et al.*, 1992], 17.6‰ [*Keeling et al.*, 1989]. However, most studies were made only with C$_3$ plants except Fung et al., and therefore they are not far from our C$_3$ estimate.

[34] BETHY online (as well as *Lloyd and Farquhar* [1994]) deviates from measurements of δ^{13}C source signature, δ_{bio}^{13}C, of *Miller et al.* [2003] (Figure 7), which are recalculated estimates of *Bakwin et al.* [1998]. (We plotted as well all model studies included in the comparison of *Miller et al.* [2003], namely *Lloyd and Farquhar* [1994], *Fung et al.* [1997], and N. S. Suits et al. (Seasonal and spatial variations in carbon isotopic ratios of plant biomass, terrestrial CO$_2$ fluxes and atmospheric CO$_2$, submitted to *Global Biogeochemical Cycles*, 2003) (hereinafter referred to as Suits et al., submitted manuscript, 2003).) Because of the lack of a full carbon cycle (but also transported fossil fuel emissions and other factors), the terrestrial isotopic signature, δ_{bio}^{13}C, is calculated here as:

$$\delta_{bio}^{13}C = \frac{-7.9 - \Delta_A^{13}C}{1 + \Delta_A^{13}C/1000}, \tag{30}$$

i.e., with an atmospheric δ^{13}C value of −7.9‰ versus VPDB-CO$_2$ which is the annual northern hemispheric mean of *Bakwin et al.* [1998]. This formulation assumes that the respiration source has the same signature as assimilation which is not true because of the fossil fuel input (so called ^{13}C Suess effect). Equation (30) and the lack of a closed carbon cycle in our model are shortcomings in the comparison but should not alter the qualitative results. However, we cannot stretch this comparison too much without including a full δ^{13}C-cycle. ECHAM/BETHY shows slightly enriched values below 35°N and lighter values in the high latitudes than the measurements (for the description of the numbers see Appendix A). *Miller et al.* [2003] and *Bakwin et al.* [1998] attributed the heavier values of *Lloyd and Farquhar* [1994] to the C$_4$ distribution used by Lloyd and Farquhar. (Bakwin et al. used the same argument for *Fung et al.* [1997].) We have a different C$_4$ distribution than Lloyd and Farquhar, but one can see in

Figures 6b and 6c that the ^{13}C discrimination of both models is very similar between 30° and 40°N for C$_3$ and C$_4$ plants together but very different for C$_3$ plants only. So the difference need not come only from the difference in C$_4$ distribution. At high latitudes, we already noted the small assimilation values of ECHAM/BETHY as well as the high c_c values.

3.5. Water Isotopes

[35] Apart from the CO$_2$ fluxes and their interdependent variables, δ^{18}O-CO$_2$ is mainly determined by the isotopic composition of the water pools. The water isotope module (WFRAC) has been extensively tested, so we focus here on the north−south gradient, which will in turn determine the latitudinal distribution of δ^{18}O-CO$_2$. We used stations of the Global Network of Isotopes in Precipitation (GNIP) of the International Atomic Energy Agency (IAEA) and the World Meteorological Organization (WMO) (see Global Network of Isotopes in Precipitation: The GNIP database, available at http://isohis.iaea.org) (details in Appendix A) and calculated the mean precipitation weighted annual average. In Figure 8 are shown the GNIP values (filled circles) together with the ECHAM annual means at the same stations (open circles). A standard deviation of around 10‰ refers to the GNIP values. The solid line in Figure 8 is the latitudinal mean of ECHAM land grid points, because most GNIP stations are on land and we are interested in the CO^{18}O fluxes of the terrestrial biosphere. One can see that ECHAM works very well at most stations, not considering the outliers in the measurements. We showed in an earlier publication [*Cuntz et al.*, 2002] that ECHAM simulates equally well the east-west gradient in Eurasia. ECHAM follows nicely the dip at 15°S resulting from the Intertropical Convergence Zone (ITCZ). However, it has a slight tendency to weakly overestimate the annual values.

3.6. Nighttime Terrestrial Source Signature

[36] The CO^{18}O module (OFRAC) uses soil water isotopic composition, not the composition of rain, to calculate soil CO^{18}O fluxes. The soil acts as an integrator of rain, damping the sometimes large seasonal cycle of δ^{18}O-H$_2$O. ECHAM uses a soil bucket model for water, which almost totally erases the seasonal cycle. The soil bucket model has only one soil layer for water. (ECHAM uses more than one soil layer for other variables like temperature.) This could already be seen in the apparent soil discrimination of Figure 2. We assess this damping effect further with CO$_2$ and δ^{18}O-CO$_2$ measurements, made in or above canopies. With the method developed by *Keeling* [1961], known as "Keeling plot", many studies have attempted to investigate the carbon isotope composition of CO$_2$ fluxes. One of the major assumptions of the Keeling plot is that the single source does not change during the period of investigation (neither should the background mixing ratio). For δ^{13}C, this can be assumed with confidence during night, but it is a priori not true for δ^{18}O-CO$_2$, because temperature changes over the course of the night and therefore the equilibrium fractionation between water and CO$_2$ changes as well (see equation (8)). There are other factors, such as the invasion effect which make a Keeling plot a priori unusable for δ^{18}O. These factors often give a curved appearance to δ^{18}O Keeling plots. In any case, one sometimes finds very 'good'
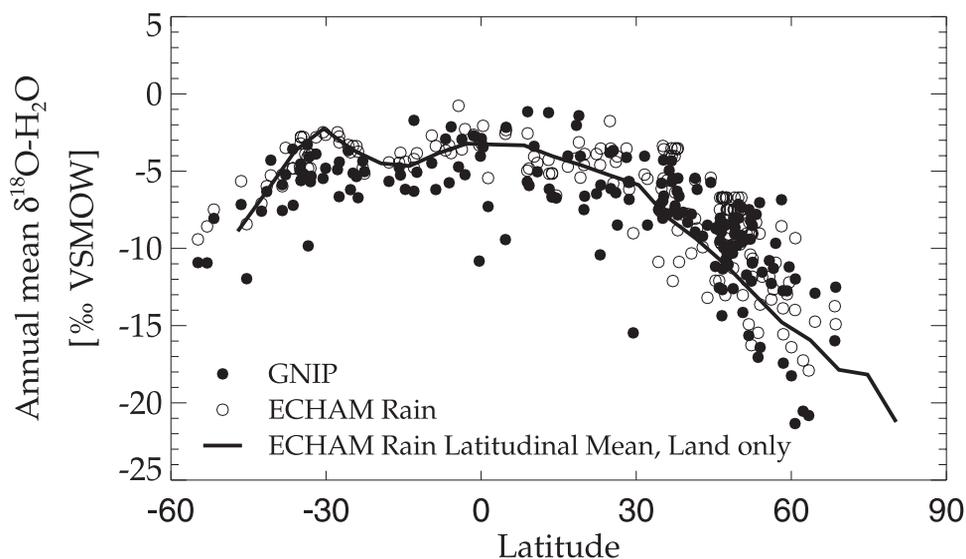
Figure 8. Annual mean values of the isotopic composition of rain from GNIP (closed circles) compared to the water isotope module (WFRAC) of ECHAM (open circles). The latitudinal mean of all land points (line) is given as an integrated comparison measure.

Keeling plots, i. e., with high correlation coefficient, and the measurements lying on a straight line. It is possible that this is due to compensating effects, because the equilibration fraction tends to heavier values over the course of the night (with decreasing temperatures, equation (8)) and the invasion effect tends to lighter values because of increasing influence (with increasing CO_2 mixing ratios, equation (12)). However, it is unlikely that these effects exactly cancel. Rather, these effects should be negligible in situations with 'good' Keeling plots. We therefore queried the database of the Biosphere-Atmosphere Stable Isotope Network (BASIN) of the Global Change and Terrestrial Ecosystem core project (GCTE) Focus 1 [*Pataki et al.*, 2003] in which we found 2470 data points of ecosystem CO_2 and $\delta^{18}O$-CO_2 measurements. We updated the measurements of French Guiana (N. Buchmann, personal communication, 2001), added data of Australia, Brazil and Cameroon (J. Lloyd, personal communication, 2001), and incorporated measurements from Russia [*Langendörfer et al.*, 2002; *Styles et al.*, 2002b] (details in Appendix A). Table A3 lists all measurement sites, along with the associated BETHY plant functional type number. We found 54 'good' ($r^2 > 0.7$) nighttime Keeling plots (using reduced major axis regression, also known as geometric mean regression). We ran our model (without invasion) for three consecutive days each month acquiring CO_2 and $\delta^{18}O$-CO_2 values each 40 minutes in the lowest model layer (about 30 meter height). We then produced Keeling plots from all nights on each grid point, and selected only Keeling plots with 'good' correlations ($r^2 > 0.9$). Taking the same coordinates as the measured Keeling plots (moving to adjacent grid cells if necessary) gave 503 individual source signature estimates in the model (out of 1110 for all stations, i.e., about half of the Keeling plots in our model were usable and the effect of source signature change negligible). We further grouped the stations according to BETHY plant functional types. The result is shown in Figure 9. If there is more than one Keeling plot, the standard deviation is plotted as an error bar at the error-weighted mean value. We take the lowest layer in ECHAM/

BETHY, which is not really a canopy air space, however. Except for C_3 short grasses, stations which correspond to a given plant functional type are either single stations or all lie around the same latitude band. So ECHAM/BETHY looks quite uniform in each plant type with small error margins. The comparison is not very enlightening because of the lack of suitable measurements in which the discussed effects are not present. In summer, nighttime temperature drifts are important, and in winter, high CO_2 mixing ratios amplify the invasion effect so that no 'good' Keeling plot can be found. Keeling plots assume entrainment of the trace gas only in the vertical, with constant signature. However, measurements are also influenced by horizontal entrainment; not constant signature should give a bend look to the Keeling plots and are discarded in the analysis. We plotted therefore in Figure 9 the signature of the source flux in ECHAM/BETHY as well (dashed line) to illustrate that the Keeling plots do not always give exactly the source signature (theoretically, they should be equal). That is why we constructed Keeling plots in our model to match as closely as possible the observational constraints. What can clearly be seen in Figure 9 is that BETHY online shows almost no seasonal cycle in the isotopic source composition. The small seasonal cycle of the water isotopes in soil is entirely cancelled out (or even overshoot) by the temperature difference between summer and winter. The sites of the BETHY plant functional types 5, 9 and 11 lie almost entirely in the northern hemisphere (except Wagga Wagga in Australia). Here BETHY online shows lower values for the source isotopic composition during the summer months. A bucket model seems to be too crude to simulate well the influence of respiration on $\delta^{18}O$-CO_2 in canopies.

4. Discussion

[37] There are two ominous results in the preceding section: the low assimilation values in high northern latitudes and the unchanging source signature of respired CO_2. We will further on summarize the above results and discuss these two points.
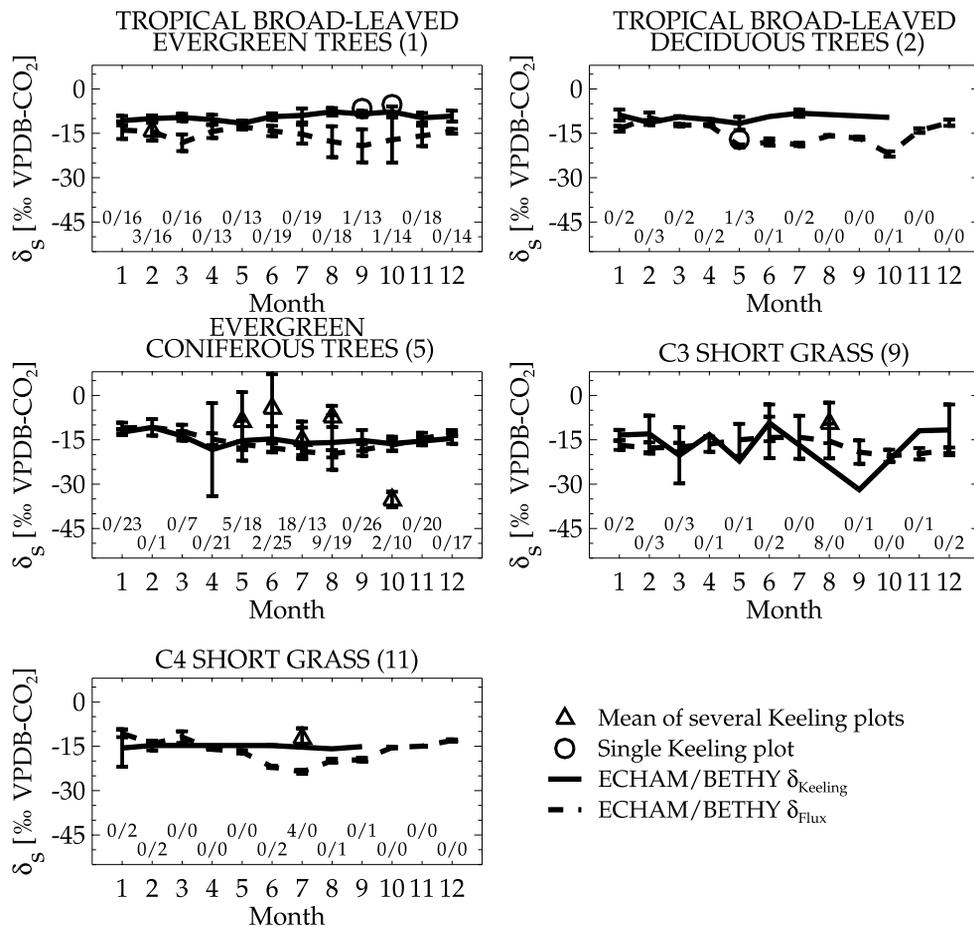
Figure 9. The isotopic signature of the nighttime respiration δ^{18}O-CO$_2$ source derived from "Keeling plots". Triangles are the mean of several Keeling-plot-derived source signatures at the given BETHY plant functional type at one or several stations. The error bar is the standard deviation of the different source estimates. Circles instead signify a single Keeling plot. The errors of single Keeling plots are all on the order of the size of the circles, and therefore no error bars are plotted to single Keeling plot values. The solid line connects the mean of the Keeling-plot-derived values in BETHY online. Here as well, an error bar is associated if more than one Keeling plot estimate exists. The numbers in each plot are first the number of measurement Keeling plots which entered the plotted value and second the number of model Keeling plots. The dashed line is the δ^{18}O signature of the soil CO$_2$ source, calculated in BETHY online.

[38] The results of the NPP comparison are somewhat contradictory (Figure 4). The BETHY online model lies only at the 10th percentile of the 15 NPP models poleward of 60°N. On the other hand, the EMDI NPP compilation shows qualitatively the same behavior as BETHY. NPP is defined as the total photosynthetic gain minus (respiratory) losses of vegetation (per unit ground area). Many earlier estimates of NPP ignored the turnover and belowground processes, taking only above-ground NPP into account. Total NPP measurements are hard to make because below-ground processes, e.g., fine root growth and death, are not easily accessible [*Long et al.*, 1989]. Different methods are thus used to estimate total NPP from measurements of above-ground NPP, but most methods still neglect quite a number of processes. The EMDI project uses conversion factors from above-ground NPP to make its estimates. *Scurlock et al.* [2002] showed, at least for grasslands, that this method can lead to substantial errors. They state that current NPP estimates are clearly an underestimate of the

magnitude of NPP. So the NPP compilation values are likely to be too small, to a different degree for different biomes. A recent atmospheric CO$_2$ data assimilation study points in the same direction, stating that a much higher NPP in high northern latitudes is needed to match the seasonal cycle of CO$_2$ [*Kaminski et al.*, 2002]. NPP derived by Kaminski et al. is even higher than the 90th percentile of the Potsdam intercomparison. However, the results are very sensitive to, e. g., the transport model used, or the parameterization of respiration. However, the seasonal cycle of atmospheric CO$_2$ is derived from the net CO$_2$ fluxes and not from gross fluxes. We showed in Figure 5 that BETHY online under-estimates NEE amplitudes at about half of the stations compared, notably poleward of 60°N. However, the two most northern stations, Flakaliden in Sweden and Hyytiälä in Finland, are both located in young, regrowing forests so that we cannot expect BETHY online to reproduce these rather high amplitudes. It is more vexing that ECHAM/BETHY is not able to reproduce the right phase poleward of

50°N. NEE is the difference between respiration and assimilation, and these show maxima at different times of the year (normally, respiration peaks later in the year than assimilation). Different NEE phasing can be due to overestimation or underestimation of one process (or both) or the different phasing of just one process. Taking Flakaliden as an example: shifting assimilation arbitrarily so that its minimum occurs one month earlier, results in the right phase and even the right amplitude in our model compared to the eddy measurements (dotted line in Figure 5). It is therefore not clear if the results of *Kaminski et al.* [2002] are transferable to our model, i.e., that we should increase the overall productivity beyond 60°N.

[39] Another item suggesting that ECHAM/BETHY underestimates carbon fluxes in high northern latitudes is the high stomata-internal CO$_2$ mixing ratio modeled by BETHY. The estimates of *Lloyd and Farquhar* [1994] and the measurements of *Miller et al.* [2003] suggest lower c_i values poleward of 45°N. Lower c_i normally means higher assimilation. This is also true in models, but only if the model has no thresholds in the computation. BETHY calculates first a non-water-limited assimilation rate at a given c_i. This means that it takes carboxylation and electron transport limitation into account in this step. Then, it incorporates the water limitation of assimilation in the empirical formulation expressed in equation (3). The last step is to recalculate assimilation, this time with fixed stomatal conductance from the water limitation step before, adjusting c_i compatibly. Therefore c_i cannot be higher than the non-water-limited c_i, which is 0.87 c_a for C$_3$ plants and 0.67 c_a for C$_4$ plants in our model. This is much higher than laboratory measurements suggest (around 0.7 c_a for C$_3$ and 0.4 c_a for C$_4$ plants [*Boyer et al.*, 1997; *Farquhar et al.*, 1989b]) but comes from a literature survey of field measurements [*Schulze et al.*, 1994]. However, this plays a role mostly in non-water-limited cases. Reducing the non-water-limited c_i to laboratory values would bring Lloyd and Farquhar and ECHAM/BETHY very close together. However, using the non-water-limited c_i of *Schulze et al.* [1994] or of *Farquhar et al.* [1989b] does not produce large changes in assimilation. It reduces assimilation only by about 5% in our model. We point out in part 2 that we use this c_i value in order to better model the seasonal cycle of atmospheric δ^{18}O-CO$_2$. We show as well in part 2 that the seasonal cycle of CO$_2$ is rather large in the model at northern hemispheric stations, which contradicts the evidence of small assimilation at high latitudes. In this regard, the mean δ^{13}_{bio}C of the only station poleward of 50°N, Baltic Sea (2), points more in the direction of ECHAM/BETHY than in the direction of Lloyd and Farquhar, and BETHY online is very similar in this region to a recent modeling study of Suits et al. (submitted manuscript, 2003).

[40] The above points support that BETHY online calculates too little assimilation in the northern hemisphere, but it also might be the case that it is the phasing of assimilation and/or respiration which is not well represented. We exclude in the discussion the possibility that ECHAM state variables are poorly represented, like temperature or relative humidity. ECHAM takes part of the Atmospheric Model Intercomparison Project (AMIP) and is tested extensively in the framework of AMIP [e.g., *Gates et al.*, 1998]. We summarize here only the key features of ECHAM for temperature

and precipitation. *Roeckner et al.* [1996] compared ECHAM temperatures with ECWMF (European Centre for Medium-Range Weather Forecasts) re-analysis climatology and precipitation to observational estimate produced by *Legates and Wilmott* [1990]. The most apparent model error is in the upper troposphere and lower stratosphere that are both not very important for our ECHAM/BETHY simulations. Over land, model errors of more than 2° occur mainly over high mountain ranges, the Sahara and during winter in Scandinavia; all these errors only minor influence our simulations. There is a small but persistent bias to higher temperatures in the Amazon region and over the United States that could lead to higher assimilation. ECHAM/BETHY predicts moderate assimilation over these regions neglecting this bias. The leaf water isotopic composition should be influenced by this bias due to lower humidity (increased leaf water) and increased equilibration (reduced leaf water). Both effects oppose each other so that the small temperature bias should be less than the error that is e.g., introduced by taking our current leaf water formulation. *Roeckner et al.* [1996] could not find any systematic differences in precipitation northward of 10°N over land but suspect a small underestimate of precipitation over Eurasia. In the southern hemisphere, the largest errors are over the oceans and over Antarctica, regions of little interest to biosphere simulations. Precipitation over the Amazon is too large during austral summer (DJF) and too small during austral winter (JJA). Assimilation depends strongly on available soil water in BETHY, overestimating assimilation in the Amazon region during austral summer. Again, ECHAM/BETHY seems not to overestimate assimilation in the Amazon region. A definite weakness is the poor representation of the monsoon in South-East Asia leading to reduced assimilation. This can be guessed in Figure 4 by the local minima at around 30°−35°N.

[41] A second point warrants discussion in the validation of ECHAM/BETHY is the invariant signal of δ^{18}O-CO$_2$ of respiration over the course of the year. This comes from the attenuation of the δ^{18}O-H$_2$O signal with the soil bucket model used in ECHAM. This behavior is probably true for deep soil but not for the upper soil layers. *Miller et al.* [1999] proposed to take the water isotope value at around 15 cm depth to equilibrate with CO$_2$ and apply afterward an effective kinetic fractionation of −7.2‰. *Riley et al.* [2002] showed that the approach of Miller et al. gives similar values as the analytical solution of *Tans* [1998] for moderate soil moisture conditions. During longer drought periods or after rain fall, Riley et al. calculate deviations from the simple approach of up to about 5‰, with tendency to higher values. They did not include the invasion effect in the Miller et al. approach, which would converge the two calculations [*Stern et al.*, 2001]. The Miller et al. approach seems therefore very robust, especially in a global model, if one includes the invasion effect. However, Miller et al. take the water isotope value at around 15 cm depth to equilibrate with CO$_2$ whereas we have a bucket model, i.e., an integrated value over the total root zone. *Melayah et al.* [1996] measured (and modeled) the gradient in δ^{18}O-H$_2$O in the unsaturated soil layer of a clay loam (bare soil) over the course of three weeks. Surface water δ^{18}O changed during that time by about 10‰ (because of evaporation and rain) whereas soil water at 10 cm depth changed only by about

2‰ and there was almost no change at all at 50 cm depth, even during and after the rain event. So water isotopic composition varies more in reality (at the place where CO_2 equilibrates with water) than the bucket model indicates, but the variation is still much attenuated, compared to rainwater. Still, our nighttime source signature comparison (Figure 9) suggests that BETHY online calculates CO_2 source signatures a few ‰ too low, leading to lower apparent soil discrimination, especially during summer with lower soil moisture.

[42] As mentioned before, we take the high non-water-limited c_i values to better model the seasonal cycle of atmospheric δ¹⁸O-CO_2. However, the seasonal cycle of δ¹⁸O depends strongly on the phasing of the isofluxes, just as CO_2 depends on the phasing of the CO_2 fluxes. So taking high c_i values could be an overcompensation effect of the wrong apparent soil discrimination. Thus the model approach of *Riley et al.* [2002] seems a promising way to better include soil processes in δ¹⁸O-CO_2 models.

5. Conclusions

[43] ECHAM/BETHY showed its capability in simulating the different components necessary to properly estimate δ¹⁸O in atmospheric CO_2. It is very similar in NPP to the median of 15 NPP models of all different kinds. In the northern hemisphere, it departs from the median and ends more at the lower estimates of the 15 models. An NPP data compilation agrees better with the lower BETHY online NPP in these latitudes, but the compilation is potentially biased toward lower values. Maximum NEE appears too low as well at latitudes poleward of 50°N but data and model can easily be brought into agreement if one shifts assimilation or respiration by about one month. The high c_i values at high northern latitudes suggest as well that assimilation could be too low at high northern latitudes but this argument does not hold if one introduces thresholds into its computation so that two interdependent variables decouple at the introduced threshold (here assimilation and c_i). It is therefore not deducible, using the current surface data, whether the northern hemispheric CO_2 fluxes are as low as BETHY online predicts or, on the other extreme, much higher as indicated by inversion techniques. The modeled total rain isotopic composition is very similar to the observed values. ECHAM uses the simplest formulation for soil water, namely a bucket; so there is only one soil water value and hence only one soil water isotope signature. Mixing new rain into the bucket does not substantially change the bucket isotopic value. The large seasonal change in the isotopic composition of rain is almost totally damped out in the soil. Together with the seasonal cycle of temperature, this leads to almost no variation in the isotopic composition of soil-respired CO_2. CO_2 fluxes, the stomata-internal CO_2 mixing ratio and the isotopic composition of soil water are thus the main determinant of atmospheric δ¹⁸O-CO_2. In the companion paper by *Cuntz et al.* [2003] (part 2), we show that we need high c_i values to simulate the seasonal cycle of δ¹⁸O-CO_2. However, our c_i estimates are most likely too high in the northern hemisphere. Diminishing c_i in the high northern latitudes would be very counterproductive for δ¹⁸O-CO_2 and would not produce large changes in CO_2 fluxes.

However, the wrong signal of respired CO_2 could act as a compensation to the c_i effect.

[44] The presented interfacing of ECHAM and BETHY offers the possibility to study some relevant δ¹⁸O-CO_2 interactive processes in a global context much more realistic than any approach up-to-date. Simulating a daily cycle provides the capacity to study the complex timing of the different processes involved, in order to obtain $CO^{18}O$ fluxes. We have demonstrated this capability in sampling the model to obtain nighttime ''Keeling plots'' on the 40 minute time step; a mandatory time resolution to compare the model with on site measurements. The interactive nature of ECHAM/BETHY along with its short calculation time step results in an altogether much more realistic analysis for δ¹⁸O-CO_2. We further explore the potential of ECHAM/BETHY in part 2, in which we focus on the atmospheric signal.

Appendix A: Data Sets
A1.   EMDI

[45] The Ecosystem Model-Data Intercomparison project [*Olson et al.*, 2001] aims to compare model estimates of terrestrial carbon fluxes (NPP) to estimates from ground-based measurements and to improve the understanding of environmental controls on carbon allocation. It extended the work of the Global Primary Production Data Initiative (GPPDI) and compiled NPP estimates for 2523 sites. We used the 3855 so-called Class C cells that represent NPP estimates for 0.5° grid cells for which inventory, modeling, or remote-sensing tools were used to scale up the point measurements. 17 grid cells were associated with two

Table A1. Stations Used for NEE Comparison With Station Abbreviations Utilized in Figure 5[a]

ABB Site	Latitude	Longitude	Type	Reference[b]
BL Blodgett For., CA, US	38.90	−120.63	5	a
BR Braschaat, BE	51.30	4.52	4	b
DU Duke For., NC, US	35.98	−79.09	5	c
FL Flakaliden, SE	64.12	19.45	5	d
HL Howland For., ME, US	45.20	−68.74	5	e
HV Harvard For., MA, US	42.54	−72.17	4	f
HY Hyytiälä, FI	61.85	24.28	5	g
LW Little Washita, OK, US	34.96	−97.98	11	h
ME Metolius, OR, US	44.50	−121.62	5	i
PO Ponca City, OK, US	36.77	−97.13	15	j
SH Shidler, OK, US	36.93	−96.68	11	j
SKO Sky Oaks, Old, CA, US	33.37	−116.62	7	k
SKY Sky Oaks, Yng, CA, US	33.38	−116.62	7	k
SO Soroe, DK	55.49	11.65	9	l
TH Tharandt, DE	50.97	13.63	5	m
CFR Centr. For. Res., RU	56.47	32.93	5	n
VI Vielsalm, BE	50.30	6.00	4	o
WB Walker Branch, TN, US	35.96	−84.29	4	p
WE Weidenbrunnen, DE	50.15	11.87	5	q
ZO Zotino, RU	60.75	89.40	5	r

[a]The second-to-last column is the number of BETHY's plant functional type (compare Table 1).
[b]References: a, *Goldstein et al.* [2000]; b, *Janssens et al.* [2001]; c, *Lai et al.* [2002]; d, *Lindroth et al.* [1998]; e, *Hollinger et al.* [1999]; f, *Barford et al.* [2001]; g, *Markkanen et al.* [2001]; h, *Meyers* [2001]; i, *Law et al.* [2001] and *Anthoni et al.* [1999]; j, *Burba and Verma* [2001]; k, *Oechel et al.* [1998]; l, *Pilegaard et al.* [2001]; m, *Bernhofer et al.* [2003] and *Grünwald and Bernhofer* [2000]; n, *Milyukova et al.* [2002]; o, *Aubinet et al.* [2001]; p, *Baldocchi et al.* [2001]; q, *Bernhofer et al.* [2003]; r, *Lloyd et al.* [2002b] and *Shibistova et al.* [2002].

estimates for different biomes where we took the biome consistent with adjacent cells. We ended up with 3838 0.5° grid cells mainly in Australia, China, the United States, Scandinavia, Senegal and South America.

A2. FLUXNET

[46] FLUXNET is a global network of micrometeorological tower sites that use eddy covariance methods to measure the exchanges of CO_2, water vapor, and energy between terrestrial ecosystems and the atmosphere [*Running et al.*, 1999]. It builds on regional networks of tower sites: Ameriflux (South and North America), CarboEurope/Euroflux (Europe), AsiaFlux (mainly East Asia), OzFlux (Australia and New Zealand), KoFLux (Korea and Thailand), and some independent tower sites. Only Ameriflux and Euroflux data is available through the Oak Ridge National Laboratory Distributed Active Archive Center (ORNL DAAC). The data is available in half-hourly, daily, weekly, monthly, and annual time intervals for each site and year. Selected gap-filling methods were used on both u* corrected data and data that had not been corrected for u* (u* correction = correction for underestimation of carbon fluxes due to stable atmospheric stratification; u*: friction velocity). The original eddy data were processed using four methods developed by *Falge et al.* [2001a, 2001b]. The "Look-up table" method with u* corrected NEE algorithm is recommended to be the most robust method for most sites. The data for Hyytiälä in Finland was updated by T. Suni (personal communication, 2001) because of problems in winter fluxes.

A3. EUROSIBERIAN CARBONFLUX

[47] We added two eddy flux measurement forest sites in Russia from the EUROSIBERIAN CARBONFLUX project [*Milyukova et al.*, 2002; *Lloyd et al.*, 2002b; *Shibistova et al.*, 2002]. The EUROSIBERIAN CARBONFLUX project includes a combination of surface flux measurements by means of the eddy covariance technique at selected stations together with atmospheric observations from aircraft of the CO_2 mixing ratio, and other atmospheric tracers linked to the carbon cycle (carbon isotopes, N_2O, SF_6, O_2/N_2, CH_4) [*Schulze et al.*, 2002]. The eddy measurements are provided as half-hourly, u* corrected NEE estimates from which we calculated the monthly means.

[48] Table A1 provides the coordinates of all 20 FLUXNET and EUROSIBERIAN CARBONFLUX stations together with the number of BETHY's plant functional type (compare Table 1) and the abbreviations used in Figure 5.

A4. NOAA/CMDL

[49] The numbers in Figure 7 correspond to continental sampling sites of the NOAA/CMDL Cooperative Air Sampling Network. We took the same numbers for each stations as *Miller et al.* [2003], and the corresponding station names are given in Table A2.

A5. GNIP

[50] The Global Network of Isotopes in Precipitation (GNIP) of the International Atomic Energy Agency (IAEA) and the World Meteorological Organization (WMO) (see Global Network of Isotopes in Precipitation: The GNIP

Table A2. Continental Station Sites With Correspondent Numbers Used in Figure 7 to Compare With ECHAM/BETHY's $\delta^{13}_{bio}C$

	Code	Site	Latitude	Longitude
1	ASK	Assekrem, DZ	23.18	5.42
2	BAL	Baltic Sea, PL	55.50	16.67
3	BSC	Black Sea, RO	44.17	28.68
4	HUN	Hegyhatsal, HU	46.95	16.65
5	ITN	North Carolina, US	35.37	−77.39
6	KZD	Plateau Assy, KZ	44.45	77.57
7	KZM	Sary Taukam, KZ	43.25	77.88
8	LEF	Wisconsin, US	45.93	−90.27
9	NWR	Colorado, US	40.05	−105.58
10	TAP	Tae-anh Penin., KR	36.73	126.13
11	UTA	Utah, US	39.90	−113.72
12	UUM	Ulaan Uum, MN	44.45	111.10
13	WIS	Negev Desert, IL	31.13	34.88
14	WLG	Mt. Waliguan, CN	36.29	100.90

database, available at http://isohis.iaea.org) has been surveying the content of hydrogen and oxygen isotopes in precipitation since 1961. More than 550 meteorological stations in 93 countries have been collecting monthly precipitation samples for GNIP, i.e., they have been collecting monthly composite total rainfall, for tritium, deuterium and ^{18}O analysis. We filtered out 186 station records with sufficient data and calculated the precipitation weighted annual mean $\delta^{18}O\text{-}H_2O$.

A6. BASIN and Further Ecosystem Resources

[51] The Biosphere-Atmosphere Stable Isotope Network (BASIN) is an activity of the Global Change and Terrestrial Ecosystem core project (GCTE) Focus 1, which aims to improve the understanding of carbon cycle processes at the ecosystem, regional, and global scales [*Pataki et al.*, 2003].

Table A3. Stations Used for Source Signature Comparison of Respired CO_2 in Figure 9[a]

Site	Latitude	Longitude	Type
Boreas, Pine, CA	55.93	−98.62	5
Boreas, Spruce, CA	55.91	−98.51	5
Cascade, WA, US	47.32	−121.58	5
Cascade Head, OR, US	44.48	−124.10	5
Brasilia, BR	−10.57	−47.58	2
Corvallis, OR, US	44.62	−123.20	5
Konza Prairie, KS, US	39.08	−96.58	11
Lethbridge, CA	49.90	−112.60	9
Logan, UT, US	41.90	−111.82	15
Manaus, For., BR	−2.59	−60.11	1
Manaus, Pasture, BR	−2.59	−60.11	12
Mbalmayo, CM	3.51	11.50	1
Metolius, OR, US	44.48	−121.62	5
Ottawa, CA	45.32	−75.67	5
Paracou, GF	5.03	−53.00	1
Red Butte Canyon, UT, US	40.78	−111.77	4
Rondonia, For., BR	−10.08	−61.93	1
Rondonia, Pasture, BR	−10.76	−61.36	1
Santarem, For. km 64, BR	−2.86	−54.96	1
Santarem, For. km 83, BR	−3.02	−54.97	1
Santarem, Pasture, BR	−3.02	−54.96	12
Sisters, OR, US	44.25	−121.23	5
Central For. Reserve, RU	56.47	32.93	5
Wagga Wagga, AU	−35.12	147.37	9
Wind River, 500 yr, WA, US	45.82	−121.95	5
Wind River, 40 yr, WA, US	45.82	−121.95	5
Wind River, 20 yr, WA, US	45.82	−121.95	5
Zotino, RU	60.75	89.40	5

[a]The last column is the number of BETHY's plant functional type (compare Table 1).

It assembles a collection of CO$_2$ and stable isotope measurements mainly in Europe and North and South America. CO$_2$ and δ^{13}C are measured at all sites of the BASIN database but δ^{18}O-CO$_2$ measurements are rather sparse. We identified 25 sites in the database with valid δ^{18}O measurements, but for two of these sites, we did not find the appropriate ecosystem in our model. This gave 2470 data points with CO$_2$ and δ^{18}O-CO$_2$ out of the BASIN database. We updated the record of Paracou in French Guiana with 42 measurements made by N. Buchmann (personal communication, 2001). In addition, we included 93 CO$_2$ and δ^{18}O-CO$_2$ measurements made by J. Lloyd and colleagues (personal communication, 2001) in Wagga Wagga, Australia, Brasilia, Brazil [*Miranda et al.*, 1996] and Mbalmayo, Cameroon. We added as well 192 data points in Russia from the EUROSIBERIAN CARBONFLUX project described above [*Langendörfer et al.*, 2002; *Styles et al.*, 2002b]. Table A3 lists the stations, their coordinates, and the numbers of the corresponding BETHY plant functional types. Together, this gives 2797 single measurements of CO$_2$ and δ^{18}O-CO$_2$, in which we found 54 nighttime events with data appropriate for Keeling plots.

Notation

a kinetic fractionation of ^{13}C diffusion in air, equal to 4.4‰.

a_1 intercept of regression between salinity and δ^{18}O-H$_2$O of ocean surface water, equal to -16.75‰ versus VSMOW.

a_2 slope of regression between salinity and δ^{18}O-H$_2$O of ocean surface water, equal to 0.5‰ versus VSMOW.

α fractionation factor.

α_d kinetic fractionation factor of CO$_2$ in (free) air, equal to 0.9913.

α_k^W effective kinetic fractionation factor of water vapor, equal to 0.974.

α_l effective fractionation factor for CO$_2$ diffusion in and out of stomata, equal to 0.9926.

$\alpha_{l\text{-}vap}^W$ fractionation factor for H$_2^{18}$O at the water-vapor phase transition.

α_s effective fractionation factor for CO$_2$ diffusion out of soil, equal to 0.9928.

α_w effective fractionation factor of CO$_2$ crossing the air-sea interface, including hydration, equal to 1.0008.

b ^{13}C fractionation associated with carboxylation, equal to 27‰.

b_3 ^{13}C fractionation associated RUBISCO carboxylation, equal to 29‰.

b_4 ^{13}C fractionation associated PEP carboxylation, equal to -5.6‰ (at 25°C).

b_e factor linking water pressure deficit and stomatal conductance without water limitation to actual stomatal conductance.

B Bunsen solubility coefficient.

c_a CO$_2$ mixing ratio in (free) air, ppm.

c_1 renormalization constant to get biosphere in equilibrium, mol(H$_2$O) m^2 s^{-1}.

c_c CO$_2$ mixing ratio in chloroplast, ppm.

c_{cs} CO$_2$ mixing ratio at the site of isotopic CO$_2$ equilibration with water, ppm.

c_i CO$_2$ mixing ratio in stomata, ppm.

c_{i0} CO$_2$ mixing ratio in stomata without water limitation, ppm.

c_w empirical parameter representing root density, equal to 0.5 mm/hr.

D molecular diffusivity of CO$_2$ in (free) air, m^2 s^{-1}.

D_{18} molecular diffusivity of CO^{18}O in (free) air, equal to $\alpha_d D$.

δ_a δ^{18}O-CO$_2$ value of (free) air, ‰ versus VPDB-CO$_2$.

δ_{a0} global initial δ^{18}O-CO$_2$ value of (free) air in the model, ‰ versus VPDB-CO$_2$.

δ_f δ^{18}O-CO$_2$ value of CO$_2$ produced by burning processes, equal to -17.0‰ versus VPDB-CO$_2$.

δ_o δ^{18}O-CO$_2$ value of CO$_2$ equilibrated with ocean surface water, ‰ versus VPDB-CO$_2$.

δ_{bio}^{13}C δ^{13}C source signature of terrestrial biosphere, ‰ versus VPDB-CO$_2$.

Δe air vapor pressure deficit, Pa.

ΔpCO_2 air-sea partial pressure difference of CO$_2$.

Δ_A discrimination of assimilation for ^{18}O.

Δ_A^{13}C   discrimination of assimilation for ^{13}C.

Δ_A^{18}O   discrimination of assimilation for ^{18}O, equal to Δ_A.

Δ_f difference between the isotopic signature of O$_2$ (involved in combustion) and CO$_2$.

Δ_{inv} apparent discrimination of invasion.

Δ_o^{des} ocean disequilibrium or the tendency to equilibrate the difference between atmospheric and ocean dissolved CO$_2$.

Δ_o^{equ} equilibrium discrimination between ocean and atmosphere.

Δ_R apparent discrimination of soil respiration.

ϵ fractionation.

ϵ_{eq} equilibrium fractionation of CO$_2$ with water, equal to $+41.1$‰ (at 25°C).

ϵ_k^W effective kinetic fractionation of water vapor, equal to -26.0‰.

ϵ_l -7.4‰, effective fractionation factor for CO$_2$ diffusion in and out of stomata.

$\epsilon_{l\text{-}vap}^W$ fractionation for H$_2^{18}$O at the water-vapor phase transition.

ϵ_s -7.2‰, effective fractionation factor for CO$_2$ diffusion out of soil.

ϵ_w $+0.8$‰, effective fractionation factor for CO$_2$ diffusion in and out of ocean water.

E_v actual transpiration rate, mol(H$_2$O) m^2 s^{-1}.

E_{vmax} potential transpiration rate, mol(H$_2$O) m^2 s^{-1}.

f_e actual/potential evapotranspiration.

F CO$_2$ flux, mol(CO$_2$) m^2 s^{-1}.

^{18}F CO^{18}O flux, mol(CO^{18}O) m^2 s^{-1}.

F_A net assimilation rate, equal to GPP $- F_{Rleaf}$, mol(CO$_2$) m^2 s^{-1}.

F_{A0} net assimilation rate without water limitation, mol(CO$_2$) m^2 s^{-1}.

$^{18}F_A$ CO^{18}O net assimilation rate, mol(CO^{18}O) m^2 s^{-1}.

F_{bur} biomass burning CO_2 flux, equal to 3.1 GtC yr^{-1}, mol(CO_2) m^2 s^{-1}.

F_{fos} fossil fuel consumption CO_2 flux, equal to 5.8 GtC yr^{-1}, mol(CO_2) m^2 s^{-1}.

F_{inv} invasion flux; virtual CO_2 in and out of soil, mol(CO_2) m^2 s^{-1}.

$^{18}F_{inv}$ $CO^{18}O$ invasion flux out of soil, mol($CO^{18}O$) m^2 s^{-1}.

F_R biorespiration flux, equal to $F_{Rhet} + F_{Rauto} - F_{Rleaf}$, mol($CO_2$) m^2 s^{-1}.

$^{18}F_R$ $CO^{18}O$ biorespiration flux, mol($CO^{18}O$) m^2 s^{-1}.

F_{Rauto} CO_2 autotrophic respiration flux, mol(CO_2) m^2 s^{-1}.

F_{Rhet} CO_2 heterotrophic respiration flux, mol(CO_2) m^2 s^{-1}.

F_{Rleaf} CO_2 leaf (dark) respiration flux, mol(CO_2) m^2 s^{-1}.

F_{Rroot} CO_2 autotrophic respiration flux that leaves plants by roots, mol(CO_2) m^2 s^{-1}.

F_{ao} CO_2 gross air-ocean flux, mol(CO_2) m^2 s^{-1}.

F_{oa} CO_2 gross ocean-air flux, mol(CO_2) m^2 s^{-1}.

F_o CO_2 net flux between ocean and atmosphere, mol(CO_2) m^2 s^{-1}.

g_c canopy conductance, mol(CO_2) m^2 s^{-1}.

g_{c0} canopy conductance without water limitation, mol(CO_2) m^2 s^{-1}.

g_s stomatal conductance, mol(CO_2) m^2 s^{-1}.

g_s' combined stomatal plus mesophyll conductance, mol(CO_2) m^2 s^{-1}.

GPP Gross Primary Productivity, mol(CO_2) m^2 s^{-1}.

h relative humidity adjusted to leaf temperature.

h_V vegetation height, m.

J_m maximum electron transport rate at 25°C, mol(CO_2) m^{-2} s^{-1}.

k PEPcase rate constant for CO_2 at 25°C (and standard pressure), mol(CO_2) m^{-2} s^{-1}.

k_1 constant of global balance equation, ‰ yr^{-1}.

k_2 inverse of e-folding time of model equilibration, yr^{-1}.

k_H CO_2 hydration rate, s^{-1}.

$^{18}k_H$ CO_2 isotope equilibration rate with water, equal to $k_H/3$, s^{-1}.

κ soil tortuosity.

M_a conversion factor between fluxes in GtC and mixing ratios in ppm, equal to 2.122 GtC ppm^{-1}.

NPP Net Primary Productivity, equal to GPP − F_{Rauto}, mol(CO_2) m^2 s^{-1}.

Q_{10} relative change in F_{Rhet} per 10° change in (air) temperature, equal to 1.5.

r^2 coefficient of determination.

R isotope ratio.

R_a $[^{18}O]/[^{16}O]$ of (free) air.

R_f $[^{18}O]/[^{16}O]$ of combusted fossil fuel.

R^W isotope ratio of water.

R_i^W $[^{18}O]/[^{16}O]$ of xylem water, approximately equal to soil water.

R_l $[^{18}O]/[^{16}O]$ of CO_2 equilibrated with leaf water at the site of evaporation.

R_l^W $[^{18}O]/[^{16}O]$ of leaf water at the site of evaporation.

$R_l^{W(t)}$ $[^{18}O]/[^{16}O]$ of leaf water at time step t.

$R_l^{W(t-1)}$ $[^{18}O]/[^{16}O]$ of leaf water one time step before t.

R_{l-ca} effective $[^{18}O]/[^{16}O]$ of CO_2 equilibrated with leaf water, taking reduced carbonic anhydrase activity into account and using the same formulation as with full carbonic anhydrase activity.

$R_{l-cg}^{W(t)}$ Craig and Gordon steady state solution of $[^{18}O]/[^{16}O]$ of water at the site of evaporation at time t.

R_s^W $[^{18}O]/[^{16}O]$ of soil water.

R_o $[^{18}O]/[^{16}O]$ of CO_2 equilibrated with ocean surface water.

R_{vap}^W $[^{18}O]/[^{16}O]$ of water vapor.

R_{VPDB} standard isotope ratio of Vienna Pee Dee Belemnite (VPDB)-CO_2 [*Allison et al.*, 1995], equal to 2088.349077 × 10^{-6}.

R_{VSMOW} standard isotope ratio of Vienna Standard Mean Ocean Water (VSMOW) [*Baertschi*, 1976], equal to 2005.2 × 10^{-6}.

S root supply rate.

SAL salinity, g(salt) kg(water)$^{-1}$.

t time step.

T_a air temperature, °C.

τ turnover time of leaf water, equal to V_l/E_v ($\approx$3), hr.

Θ_a air-filled pore fraction of soil.

Θ_w water-filled pore fraction.

u*   friction velocity, m s^{-1}.

V_l leaf water volume.

V_m maximum carboxylation rate at 25°C, mol(CO_2) m^{-2} s^{-1}.

W_s actual soil water content, m.

$W_{s,max}$ maximal root available soil water content, m.

ζ $=(1 - h)(\epsilon_{l-vap}^W + 1)(\epsilon_k^W + 1)$.

References

Allison, C. E., R. J. Francey, and H. A. Meijer, Recommendations for the reporting of stable isotope measurements of carbon and oxygen in CO_2 gas, in *References and Intercomparison Materials for Stable Isotopes of Light Elements, IAEA-TECDOC-825*, pp. 155–162, Int. At. Energy Agency, Vienna, 1995.

Andres, R. J., G. Marland, I. Fung, and E. Matthews, A 1 × 1 distribution of carbon dioxide emissions from fossil fuel consumption and cement manufacture, 1950–1990, *Global Biogeochem. Cycles*, 10, 419–429, 1996.

Anthoni, P. M., B. E. Law, and M. H. Unsworth, Carbon and water vapor exchange of an open-canopied Ponderosa pine ecosystem, *Agric. For. Meteorol.*, 95, 151–168, 1999.

Arpe, K., L. Bengtsson, L. Dümenil, and E. Roeckner, The hydrological cycle in the ECHAM3 simulations of the atmospheric circulation, in *Global Precipitation and Climate Change*, edited by M. Desbois and F. Desalmand, pp. 361–377, Springer-Verlag, New York, 1994.

Aubinet, M., B. Chermanne, M. Vandenhaute, B. Longdoz, M. Yernaux, and E. Laitat, Long term carbon dioxide exchange above a mixed forest in the Belgian Ardennes, *Agric. For. Meteorol.*, 108, 293–315, 2001.

Baertschi, P., Absolute ^{18}O content of standard mean ocean water, *Earth Planet. Sci. Lett.*, *31*, 314–344, 1976.

Bakwin, P. S., P. P. Tans, J. W. C. White, and R. J. Andres, Measurements of carbon dioxide on very tall towers: Results of the NOAA/CMDL program, *Tellus, Ser. B*, *50*, 401–415, 1998.

Baldocchi, D., E. Falge, and K. Wilson, A spectral analysis of biosphere-atmosphere trace gas flux densities and meteorological variables across hour to multi-year time scales, *Agric. For. Meteorol.*, *107*, 1–27, 2001.

Barford, C. C., S. C. Wofsy, M. L. Goulden, J. W. Munger, E. H. Pyle, S. P. Urbanski, L. Hutyra, S. R. Saleska, D. Fitzjarrald, and K. Moore, Factors controlling long- and short-term sequestration of atmospheric CO$_2$ in a mid-latitude forest, *Science*, *294*, 1688–1691, 2001.

Bariac, T., J. Gonzalez-Dunia, N. Katerji, O. Béthenod, J. M. Bertolini, and A. Mariotti, Variabilité spatiale de la composition isotopique de l'eau (^{18}O, ^{2}H) dans le continuum sol-plante-atmosphère: 2. Approche en conditions naturelles, *Chem. Geol.*, *115*, 317–333, 1994a.

Bariac, T., J. Gonzalez-Dunia, D. Tessier, and A. Mariotti, Variabilité spatialle de la composition isotopique de l'eau (^{18}O, ^{2}H) au sein des organes des plantes aériennes: 1. Approche en conditions controlées, *Chem. Geol.*, *15*, 307–315, 1994b.

Bernhofer, C., M. Aubinet, R. Clement, A. Grelle, T. Grünwald, A. Ibrom, P. Jarvis, C. Rebmann, E.-D. Schulze, and J. D. Tenhunen, Spruce forests (Norway and Sitka spruce, including Douglas fir): Carbon and water fluxes and balances, ecological and ecophysiological determinants, in *Fluxes of Carbon, Water, and Energy of European Forests, Ecol. Stud.*, vol. 163, edited by R. Valentini et al., Springer-Verlag, New York, 2003.

Boyer, J. S., S. C. Wong, and G. D. Farquhar, CO$_2$ and water vapor exchange across leaf cuticle (epidermis) at various water potentials, *Plant Physiol.*, *114*, 185–191, 1997.

Brenninkmeijer, C. A. M., P. Kraft, and W. G. Mook, Oxygen isotope fractionation between CO$_2$ and H$_2$O, *Isot. Geosci.*, *1*, 181–190, 1983.

Burba, G. G., and S. B. Verma, Prairie growth, PAR albedo and seasonal distribution of energy fluxes, *Agric. For. Meteorol.*, *107*, 227–240, 2001.

Cernusak, L. A., J. S. Pate, and G. D. Farquhar, Diurnal variation in the stable isotope composition of water and dry matter in fruiting *Lupinus angustifolius* under field conditions, *Plant Cell Environ.*, *25*, 893–907, 2002.

Ciais, P., et al., A three dimensional synthesis study of δ^{18}O in atmospheric CO$_2$: 1. Surface fluxes, *J. Geophys. Res.*, *102*, 5857–5872, 1997a.

Ciais, P., et al., A three dimensional synthesis study of δ^{18}O in atmospheric CO$_2$: 2. Simulations with the TM2 transport model, *J. Geophys. Res.*, *102*, 5873–5883, 1997b.

Collatz, G. J., M. Ribas-Carbo, and J. A. Berry, Coupled photosynthesis-stomatal conductance model for leaves of C$_4$ plants, *Aust. J. Plant Physiol.*, *19*, 519–538, 1992.

Craig, H., and L. I. Gordon, *Deuterium and Oxygen: 18 Variations in the Ocean and the Marine Atmosphere*, Lab. di Geol. Nucl., Cons. Naz. delle Ric., Trieste, Italy, 1965.

Cramer, W., D. W. Kicklighter, A. Bondeau, B. Moore III, G. Churkina, B. Nemry, A. Ruimy, A. L. Schloss, and the participants of the Potsdam NPP Model Intercomparison, Comparing global models of terrestrial net primary productivity (NPP): Overview and key results, *Global Change Biol.*, *5*, suppl. 1, 1–15, 1999.

Cuntz, M., P. Ciais, and G. Hoffmann, Modelling the continental effect of oxygen isotopes over Eurasia, *Tellus, Ser. B*, *54*, 895–909, 2002.

Cuntz, M., P. Ciais, G. Hoffmann, C. E. Allison, R. J. Francey, W. Knorr, P. P. Tans, J. W. C. White, and I. Levin, A comprehensive global three-dimensional model of δ^{18}O in atmospheric CO$_2$: 2. Mapping the atmospheric signal, *J. Geophys. Res.*, *108*, doi:10.1029/2002JD003154, in press, 2003.

Dongmann, G., H. W. Nürnberg, H. Förstel, and K. Wagner, On the enrichment of H$_2$^{18}O in the leaves of transpiring plants, *Radiat. Environ. Biophys.*, *11*, 41–52, 1974.

Falge, E., et al., Gap filling strategies for defensible annual sums of net ecosystem exchange, *Agric. For. Meteorol.*, *107*, 43–69, 2001a.

Falge, E., et al., Gap filling strategies for longterm energy flux data sets, *Agric. For. Meteorol.*, *107*, 71–77, 2001b.

Farquhar, G. D., S. von Caemmener, and J. A. Berry, A biochemical model of photosynthesis CO$_2$ fixation in leaves of C$_3$ species, *Planta*, *149*, 78–90, 1980.

Farquhar, G. D., M. H. O'Leary, and J. A. Berry, On the relationship between carbon isotope discrimination and the intercellular carbon dioxide concentration in leaves, *Aust. J. Plant Physiol.*, *9*, 121–137, 1982.

Farquhar, G. D., J. R. Ehleringer, and K. T. Hubick, Carbon isotope discrimination and photosynthesis, *Annu. Rev. Plant Physiol. Plant Mol. Biol.*, *40*, 503–537, 1989a.

Farquhar, G. D., K. T. Hubick, A. G. Condon, and R. A. Richards, Carbon isotope fractionation and plant water-use efficiency, in *Stable Isotopes in Ecological Research*, edited by P. W. Rundel, pp. 21–40, Springer-Verlag, New York, 1989b.

Farquhar, G. D., J. Lloyd, J. A. Taylor, L. B. Flanagan, J. P. Syvertsen, K. T. Hubick, S. C. Wong, and J. R. Ehleringer, Vegetation effects on the isotope composition of oxygen in atmospheric CO$_2$, *Nature*, *363*, 439–443, 1993.

Federer, C. A., Transpirational supply and demand: plant, soil, and atmospheric effects evaluated by simulation, *Water Resour. Res.*, *18*, 355–362, 1982.

Firestone, R. B., C. M. B. V. S. Shirley, S. Y. F. Chu, and J. Zipkin, *Table of Isotopes* [book and CD-ROM], 8th ed., John Wiley, New York, 1999.

Fischer, R. A., and N. C. Turner, Plant productivity in the arid and semiarid zones, *Annu. Rev. Plant Physiol.*, *29*, 277–317, 1978.

Förstel, H., A. Putral, G. Schleser, and H. Leith, The world pattern of oxygen-18 in rain water and its importance in understanding the biogeochemical oxygen cycle, in *Isotope Ratios as Pollutant Source and Behavier Indicators*, pp. 323–344, Int. At. Energy Agency, Vienna, 1975.

Francey, R. J., and P. P. Tans, Latitudinal variation in oxygen-18 of atmospheric CO$_2$, *Nature*, *327*, 495–497, 1987.

Fung, I., et al., Carbon 13 exchanges between the atmosphere and biosphere, *Global Biogeochem. Cycles*, *11*, 507–533, 1997.

Gates, W. L., et al., An overview of the results of the Atmospheric Model Intercomparison Project (AMIP I), *Bull. Am. Meteorol. Soc.*, *73*, 1962–1970, 1998.

Gillon, J., and D. Yakir, Internal conductance to CO$_2$ diffusion and C^{18}OO discrimination in C$_3$ leaves, *Plant Physiol.*, *123*, 201–213, 2000a.

Gillon, J., and D. Yakir, Naturally low carbonic anhydrase activity in C$_4$ and C$_3$ plants limits discrimination against C^{18}OO during photosynthesis, *Plant Cell Environ.*, *23*, 903–915, 2000b.

Gillon, J., and D. Yakir, Influence of carbonic anhydrase activity in terrestrial vegetation on the ^{18}O content of atmospheric CO$_2$, *Science*, *291*, 2584–2587, 2001.

Goldstein, A. H., N. E. Hultman, J. M. Fracheboud, M. R. Bauer, J. A. Panek, M. Xu, Y. Qi, A. B. Guenther, and W. Baugh, Effects of climate variability on the carbon dioxide, water, and sensible heat fluxes above a ponderosa pine plantation in the Sierra Nevada (CA), *Agric. For. Meteorol.*, *101*, 113–129, 2000.

Grünwald, T., and C. Bernhofer, Data gap filling with regression modelling, in *Forest Ecosystem Modelling, Upscaling and Remote Sensing*, edited by R. J. M. Ceulemans et al., pp. 61–67, SPB Acad., The Hague, 2000.

Gurney, K. R., et al., Towards robust regional estimates of annual mean CO$_2$ sources and sinks, *Nature*, *415*, 626–630, 2002.

Hao, W. M., and M.-H. Liu, Spatial and temporal distribution of tropical biomass burning, *Global Biogeochem. Cycles*, *8*, 495–503, 1994.

Hoffmann, G., M. Werner, and M. Heimann, Water isotopes module of the ECHAM atmospheric general circulation model: A study on timescales from days to several years, *J. Geophys. Res.*, *103*, 16,871–16,896, 1998.

Hoffmann, G., V. Masson, and J. Jouzel, Stable water isotopes in atmospheric general circulation models, *Hydrol. Processes*, *14*, 1385–1406, 2000.

Hollinger, D. Y., S. M. Goltz, E. A. Davidson, J. T. Lee, K. Tu, and H. T. Valentine, Seasonal patterns and environmental control of carbon dioxide and water vapour exchange in an ecotonal boreal forest, *Global Change Biol.*, *5*, 891–902, 1999.

Janssens, I. A., A. S. Kowalski, and R. Ceulemans, Intercomparison of forest floor CO$_2$ efflux estimates by eddy correlation and a chamber-based empirical model, *Agric. For. Meteorol.*, *106*, 61–69, 2001.

Jones, H. G., *Plants and Microclimate*, Cambridge Univ. Press, New York, 1983.

Kaminski, T., W. Knorr, P. J. Rayner, and M. Heimann, Assimilating atmospheric data into a terrestrial biosphere model: A case study of the seasonal cycle, *Global Biogeochem. Cycles*, *16*, 1066–1082, 2002.

Keeling, C. D., The concentration and isotopic abundances of carbon dioxide in rural and marine air, *Geochim. Cosmochim. Acta*, *24*, 277–298, 1961.

Keeling, C. D., R. B. Bacastow, A. F. Carter, S. C. Piper, T. P. Whorf, M. Heimann, W. G. Mook, and H. Roeloffzen, A three-dimensional model of atmospheric CO$_2$ transport based on observed winds: 1. Analysis on observational data, in *Aspects of Climate Variability in the Pacific and the Western Americas, Geophys. Monogr. Ser.*, vol. 55, edited by D. H. Peterson, pp. 165–236, AGU, Washington, D. C., 1989.

Kicklighter, D. W., A. Bondeau, A. L. Schloss, J. Kaduk, A. D. McGuire, and the participants of the Potsdam NPP Model Intercomparison, Comparing global models of terrestrial net primary productivity (NPP): Global pattern and differentiation by major biomes, *Global Change Biol.*, *5*, suppl. 1, 16–24, 1999.

Knorr, W., Satellite remote sensing and modelling of the global CO$_2$ exchange of land vegetation: A synthesis study (in German), Ph.D. thesis, Max-Planck-Inst. für Meteorol., Hamburg, Germany, 1997.

Knorr, W., Annual and interannual CO$_2$ exchange of the terrestrial biosphere: Process-based simulations and uncertainties, *Global Ecol. Biogeogr.*, *9*, 225–252, 2000.

Knorr, W., and M. Heimann, Impact of drought stress and other factors on seasonal land biosphere CO$_2$ exchange studied through an atmospheric tracer transport model, *Tellus, Ser. B, 47*, 471–489, 1995.

Knorr, W., and M. Heimann, Uncertainties in global terrestrial biosphere modeling: 1. A comprehensive sensitivity analysis with a new photosynthesis and energy balance scheme, *Global Biogeochem. Cycles, 15*, 207–225, 2001a.

Knorr, W., and M. Heimann, Uncertainties in global terrestrial biosphere modeling: 2. Global constraints for a process-based vegetation model, *Global Biogeochem. Cycles, 15*, 227–246, 2001b.

Lai, C. T., G. Katul, J. Butnor, D. Ellsworth, and R. Oren, Modelling nighttime ecosystem respiration by a constrained source optimization method, *Global Change Biol., 8*, 124–141, 2002.

Langendörfer, U., M. Cuntz, P. Ciais, P. Peylin, T. Bariac, I. Milyukova, O. Kolle, T. Naegler, and I. Levin, Modelling of biospheric CO$_2$ gross fluxes via oxygen isotopes in a spruce forest canopy: A ^{222}Rn calibrated box model approach, *Tellus, Ser. B, 54*, 476–496, 2002.

Law, B. E., P. Thornton, J. Irvine, S. Van Tuyl, and P. M. Anthoni, Carbon storage and fluxes in ponderosa pine forests at different developmental stages, *Global Change Biol., 7*, 755–777, 2001.

Leemans, R., and W. Cramer, The IIASA climate database for mean monthly values of temperature, precipitation and cloudiness on a global terrestrial grid, *Tech. Rep. RR-19-81*, Int. Inst. of Appl. Syst. Anal., Laxenburg, Austria, 1991.

Legates, D. R., and C. J. Wilmott, Mean seasonal and spatial variability in gauge corrected global precipitation, *J. Climatol., 10*, 111–127, 1990.

Lindroth, A., and S. Halldin, Numerical analysis of pine forest evaporation and surface resistance, *Agric. For. Meteorol., 38*, 59–79, 1986.

Lindroth, A., A. Grelle, and A. S. Moren, Long-term measurements of boreal forest carbon balance reveal large temperature sensitivity, *Global Change Biol., 4*, 443–450, 1998.

Lloyd, J., and G. D. Farquhar, ^{13}C discrimination during CO$_2$ assimilation by the terrestrial biosphere, *Oecologia, 99*, 201–215, 1994.

Lloyd, J., and J. A. Taylor, On the temperature dependance of soil respiration, *Funct. Ecol., 8*, 315–323, 1994.

Lloyd, J., et al., A trace gas climatology above Zotino, central Siberia, *Tellus, Ser. B, 54*, 749–767, 2002a.

Lloyd, J., O. Shibistova, D. Zolothukhine, O. Kolle, A. Arneth, J. Styles, N. M. Tchebakova, and E.-D. Schulze, Seasonal and annual variations in the photosynthetic productivity and carbon balance of a central Siberian pine forest, *Tellus, Ser. B, 54B*, 590–610, 2002b.

Long, S. P., E. G. Moya, S. K. Imbamba, A. Kamnalrut, M. T. F. Piedade, J. M. O. Scurlock, Y. K. Shen, and D. O. Hall, Primary productivity of natural grass ecosystems of the tropics: A reappraisal, *Plant Soil, 115*, 155–166, 1989.

Majoube, M., Fractionnement en oxygene-18 et en deuterium entre l'eau et sa vapeur, *J. Chim. Phys., 58*, 1423–1436, 1971.

Markkanen, T., Ü. Rannik, P. Keronen, T. Suni, and T. Vesala, Eddy covariance fluxes over a boreal Scots pine forest, *Boreal Environ. Res., 6*, 65–78, 2001.

Marland, G., R. J. Andres, T. A. Boden, C. Johnston, and A. Brenkert, Global, regional and national CO$_2$ emission estimates from fossil fuel burning, cement production and gas flaring: 1751–1996, *Data Rep. ORNL NDP-030*, Carbon Dioxide Inf. Anal. Cent., Oak Ridge Natl. Lab., Oak Ridge, Tenn., 1998. (Revised March 1999.).

Meentemeyer, V., Macroclimate and lignin control of litter decomposition rates, *Ecology, 59*, 465–472, 1978.

Melayah, A., L. Bruckler, and T. Bariac, Modeling the transport of water stable isotopes in unsaturated soils under natural conditions: 2. Comparison with field experiments, *Water Resour. Res., 32*, 2055–2065, 1996.

Merlivat, L., and J. Jouzel, Global climatic interpretation of the deuterium-oxygen 18 relationship for precipitation, *J. Geophys. Res., 84*, 5029–5033, 1979.

Meyers, T. P., A comparison of summertime water and CO$_2$ fluxes over rangeland for well watered and drought conditions, *Agric. For. Meteorol., 106*, 205–214, 2001.

Miller, J. B., D. Yakir, J. W. C. White, and P. P. Tans, Measurement of ^{18}O/^{16}O in the soil-atmosphere CO$_2$ flux, *Global Biogeochem. Cycles, 13*, 761–774, 1999.

Miller, J. B., P. P. Tans, J. W. C. White, T. J. Conway, and B. W. Vaughn, The atmospheric signal of terrestrial carbon isotopic discrimination and its implication for partitioning carbon fluxes, *Tellus, Ser. B, 55*, 197–206, 2003.

Milyukova, I. M., O. E. Kolle, A. B. Varlagin, N. N. Vygodskaya, E.-D. Schulze, and J. Lloyd, Carbon balance of a southern Taiga spruce stand in European Russia, *Tellus, Ser. B, 54*, 429–442, 2002.

Miranda, A. C., H. S. Miranda, J. Lloyd, J. Grace, R. J. Francey, P. Riggan, and J. Brass, Fluxes of carbon dioxide and water vapour over cerrado vegetation in Central Brazil: An analysis using eddy correlation and stable isotope techniques, *Plant Cell Environ., 20*, 315–328, 1996.

Modellbetreuungsgruppe, The ECHAM3 atmospheric general circulation model, *Tech. Rep. 6*, Dtsch. Klimarechenzent., Hamburg, Germany, 1994.

Monteith, J. L., Climate and the efficiency of crop production in Britain, *Philos. Trans. R. Soc. London, Ser. B, 281*, 277–294, 1977.

Oechel, W. C., G. L. Vourlitis, S. J. Hastings, R. P. Ault, and P. Bryant, The effects of water table manipulation and elevated temperature on the net CO$_2$ flux of wet sedge tundra ecosystems, *Global Change Biol., 4*, 77–90, 1998.

Olson, R. J., J. M. O. Scurlock, S. D. Prince, D. L. Zheng, and K. R. Johnson (Eds.), NPP multi-biome: NPP and driver data for ecosystem model, data intercomparison, http://www.daac.ornl.gov/, Oak Ridge Natl. Lab. Distrib. Active Arch. Cent., Oak Ridge, Tenn., 2001.

Pataki, D. E., J. R. Ehleringer, L. B. Flanagan, D. Yakir, D. R. Bowling, C. Still, N. Buchmann, J. Kaplan, and J. A. Berry, The application and interpretation of keeling plots in terrestrial carbon cycle research, *Global Biogeochem. Cycles, 17*, 1022–1036, 2003.

Peylin, P., The composition of ^{18}O in atmospheric CO$_2$: A new tracer to estimate global photosynthesis (in French), Ph.D. thesis, Univ. Paris VI, Pierre et Marie Curie, 1999.

Peylin, P., P. Ciais, P. P. Tans, K. Six, J. A. Berry, and A. S. Denning, ^{18}O in atmospheric CO$_2$ simulated by a 3-D transport model: A sensitivity study to vegetation and soil fractionation factors, *Phys. Chem. Earth, 21*, 463–469, 1997.

Peylin, P., P. Ciais, A. S. Denning, P. P. Tans, J. A. Berry, and W. C. White, A three-dimensional study of δ^{18}O in atmospheric CO$_2$: Contributin of different land ecosystems, *Tellus, Ser. B, 51*, 642–667, 1999.

Pilegaard, K., P. Hummelshoj, N. O. Jensen, and Z. Chen, Two years of continuous CO$_2$ eddy-flux measurements over a Danish beech forest, *Agric. For. Meteorol., 107*, 29–41, 2001.

Quay, P. D., B. Tilbrook, and C. S. Wong, Oceanic uptake of fossil fuel CO$_2$: Carbon-13 evidence, *Science, 256*, 74–79, 1992.

Raich, J. W., and C. S. Potter, Global patterns of carbon dioxide emissions from soils, *Global Biogeochem. Cycles, 9*, 23–36, 1995.

Raich, J. W., and W. H. Schlesinger, The global carbon dioxide flux in soil respiration and its relationship to vegetation and climate, *Tellus, Ser. B, 44*, 81–99, 1992.

Riley, W. J., C. J. Still, M. S. Torn, and J. A. Berry, A mechanistic model of H$_2^{18}$O and C^{18}OO fluxes between ecosystems and the atmosphere: Model description and sensitivity analyses, *Global Biogeochem. Cycles, 16*, 1095–1108, 2002.

Roche, C., Interactions biosphere-atmosphere aux echelles locales et composition isotopique (^{13}C, ^{18}O) du CO$_2$ atmospherique: Application a la foret landaise (in French), Ph.D. thesis, Univ. Paris VI, Pierre et Marie Curie, 1999.

Roeckner, E., et al., Simulation of the present-day climate with the ECHAM model: Impact of model physics and resolution, *Tech. Rep. 93*, Max-Planck-Inst. für Meteorol., Hamburg, Germany, 1992.

Roeckner, E., K. Arpe, L. Bengtsson, M. Christoph, M. Clausen, L. Dümenil, M. Esch, M. Giorgetta, U. Schlese, and U. Schulzweida, The atmospheric general circulation model ECHAM-4: Model description and simulation of present-day climate, *Tech. Rep. 218*, Max-Planck-Inst. für Meteorol., Hamburg, Germany, 1996.

Running, S. W., D. D. Baldocchi, W. B. Cohen, S. T. Gower, D. P. Turner, P. S. Bakwin, and K. A. Hibbard, A global terrestrial monitoring network intergrating tower fluxes with ecosystem modeling and EOS satellite data, *Remote Sens. Environ., 70*, 108–127, 1999.

Schulze, E.-D., Carbon dioxide and water exchange in response to drought in the atmosphere and in the soil, *Annu. Rev. Plant Physiol., 13*, 127–141, 1986.

Schulze, E.-D., N. C. Turner, T. Gollan, and K. A. Shakel, Stomatal response to air humidity and to soil drought, in *Stomatal Function*, edited by E. Zeiger, G. Farquhar, and I. Cowan, pp. 311–321, Stanford Univ. Press, Stanford, Calif., 1987.

Schulze, E.-D., F. M. Kelliher, C. Lloyd, and R. Leuning, Relationships among maximum stomatal conductance, ecosystem surface conductance, carbon assimilation rate, and plant nitrogen nutrition: A global ecology scaling exercise, *Annu. Rev. Ecol. Syst., 25*, 629–660, 1994.

Schulze, E.-D., N. N. Vygodskaya, N. Tschebakova, C. I. Czimczik, D. Kozlov, J. Lloyd, D. Mollicone, E. Myachkova, K. Sidorov, A. Varlagin, and C. Wirth, The Eurosiberian transect: An introduction to the experimental region, *Tellus, Ser. B, 54*, 421–428, 2002.

Scurlock, J. M. O., K. Johnson, and R. J. Olson, Estimating net primary productivity from grassland biomass dynamics measurements, *Global Change Biol., 8*, 736–753, 2002.

Sellers, P. J., Canopy reflectance, photosynthesis, and transpiration, *Int. J. Remote Sens., 6*, 1335–1372, 1985.

Shibistova, O., J. Lloyd, G. Zrazhewskaya, A. Arneth, O. Kolle, N. Astrakhantceva, I. Shijneva, A. Knohl, and J. Schmerler, Ecosystem respiration budget for a *pinus sylvestris* stand in central Siberia, *Tellus, Ser. B, 54*, 552–567, 2002.

Stern, L. A., W. T. Baisden, and R. Amundson, Processes controlling the oxygen isotope ratio of soil CO_2: Analytical and numerical modeling, *Geochim. Cosmochim. Acta*, *63*, 799–814, 1999.

Stern, L. A., R. Amundson, and W. T. Baisden, Influence of soils on oxygen isotope ratio of atmospheric CO_2, *Global Biogeochem. Cycles*, *15*, 753–760, 2001.

Stryer, L., *Biochemistry*, W. H. Freeman, New York, 1981.

Styles, J. M., J. Lloyd, D. Zolotukhin, K. A. Lawton, N. M. Tschebakova, R. J. Francey, A. A. Arneth, D. Salamakho, O. Kolle, and E.-D. Schulze, Estimates of regional surface CO_2 exchange and carbon and oxygen isotope discrimination during photosynthesis from concentration profiles in the atmospheric boundary layer, *Tellus, Ser. B*, *54*, 768–783, 2002a.

Styles, J. M., et al., Soil and canopy CO_2, $^{13}CO_2$, H_2O and sensible heat flux partitions in a forest canopy inferred from concentration measurements, *Tellus, Ser. B*, *54*, 655–676, 2002b.

Takahashi, T., R. H. Wanninkhof, R. A. Feely, R. F. Weiss, D. W. Chipman, N. Bates, J. Olafsson, C. Sabine, and S. C. Sutherland, Net sea-air CO_2 flux over the global oceans: An improved estimate based on the sea-air pCO_2 difference, paper presented at 2nd International Symposium, CO_2 in the Oceans, Cent. for Global Environ. Res., Tsukuba, Japan, 1999.

Tans, P. P., Oxygen isotopic equilibrium between carbon dioxide and water in soils, *Tellus, Ser. B*, *50*, 163–178, 1998. (Correction, *Tellus, Ser. B*, *50*, 400, 1998.)

Tans, P. P., J. A. Berry, and R. F. Keeling, Oceanic ^{13}C data: A new window on CO_2 uptake by the oceans, *Global Biogeochem. Cycles*, *7*, 353–368, 1993.

Turner, N. C., Adaptation to water deficits: A changing perspective, *Aust. J. Plant Physiol.*, *13*, 338–342, 1986.

Vogel, J. C., P. M. Grootes, and W. G. Mook, Isotopic fractionation between gaseous and dissolved carbon dioxide, *Z. Phys.*, *230*, 225–238, 1970.

Wanninkhof, R., Relationship between wind speed and gas exchange over the ocean, *J. Geophys. Res.*, *97*, 7373–7382, 1992.

Werner, M., M. Heimann, and G. Hoffmann, Isotopic composition and origin of polar precipitation in present and glacial climate simulations, *Tellus, Ser. B*, *53*, 53–71, 2001.

White, J. W. C., The climatic significance of D/H ratios in white pine in the northeastern United States, Ph.D. thesis, Columbia Univ., New York, 1983.

Yakir, D., Oxygen-18 of leaf water: A crossroad for plant-associated isotopic signals, in *Stable Isotopes: Integration of Biological, Ecological and Geochemical Processes*, edited by H. Griffiths, chap. 10, pp. 147–168, βIOS Sci., Oxford, England, 1998.

Yakir, D., and L. S. L. Sternberg, The use of stable isotopes to study ecosystem gas exchange, *Oecologia*, *123*, 297–311, 2000.

———————————

P. Ciais, M. Cuntz, and G. Hoffmann, Laboratoire des Sciences du Climat et de l'Environnement, Unité Mixte de CNRS/CEA, Bât. 709, L'Orme des Merisiers, F-91191 Gif-sur-Yvette Cedex, France. (ciais@lsce.saclay.cea.fr; cuntz@lsce.saclay.cea.fr; hoffmann@lsce.saclay.cea.fr)

W. Knorr, Max-Planck-Institut für Biogeochemie, Carl-Zeiss-Promenade 10, D-07745 Jena, Germany. (wknorr@bgc-jena.mpg.de)